

Melting of a dry peridotite at high pressures and basalt magma genesis

EIICHI TAKAHASHI

*Institute for Thermal Spring Research
Okayama University, Misasa, Tottori-ken, 682-02, Japan*

AND IKUO KUSHIRO

*Geological Institute, Faculty of Science
Tokyo University, Bunkyo-ku, Tokyo, 113, Japan*

Abstract

The solidus of a spinel lherzolite (HK66) was determined under dry conditions through the pressure range 1 atm to 30 kbar. It was found that the solidus comprises three curves corresponding to subsolidus mineral assemblages with cusps at about 11 and 26 kbar. In order to determine the composition of melt coexisting with peridotite, a thin layer of basalt was sandwiched between compressed blocks of powdered peridotite minerals and then was equilibrated with its host at melting temperatures. A time study at 15 kbar and 1300°C (25°C above the solidus) showed that the basalt melt embedded in the peridotite was completely homogenized with the partial melt in the peridotite matrix within 24 hours. The composition of melt formed along the solidus of the peridotite is a quartz tholeiite at 5 kbar, an olivine tholeiite similar to mid-ocean ridge basalt (MORB) at 8 and 10 kbar, an alkali-olivine basalt between 15 and 20 kbar, and an alkali picrite above 25 kbar. The role of K₂O in the melting was specifically investigated by adding 20 wt.% potassium feldspar to the starting peridotite. The solidus of the K-rich peridotite is 70° and 150°C lower than that of the original peridotite at 20 and 30 kbar, respectively. Its extension may intersect with the normal oceanic geotherm at a pressure between 30 and 50 kbar. The melts are leucite phonolitic at the solidus of the K-rich peridotite and change gradually to the composition of the alkali picrite at the solidus of the original peridotite. A hypothesis of shallow depth origin for MORBs is supported by the fact that the composition of melt formed near the solidus at 8 kbar (16 wt.% Al₂O₃, 11 wt.% CaO, 9 wt.% MgO) plots in the middle of the MORB's cluster in the normative projections. The olivine-liquid Fe/Mg partition coefficient, $K_D = (\text{Fe}/\text{Mg})^{\text{ol}}/(\text{Fe}/\text{Mg})^{\text{liq}}$ is given by $K_D = 0.30 + 0.002 P$ (kbar) in the pressure range 1 atm to 35 kbar. Judging from the K_D values, most previously reported glass compositions in peridotite melting experiments are significantly modified by the overgrowth effect of residual solids.

Introduction

It is a well-accepted hypothesis that terrestrial basalt magmas are formed by partial melting of peridotite in the upper mantle (Bowen, 1928; Ringwood, 1975; Yoder, 1976). Both depth and degree of partial melting are believed to be important in producing the diversity of basalt magma types (Kushiro and Kuno, 1963; Green and Ringwood, 1967a; O'Hara, 1965, 1968; Ito and Kennedy, 1968). Numerous experiments have been attempted to determine the compositions of liquids produced by partial melting of peridotite under various pressure-temperature conditions. There has been a debate, however, among experimental petrologists on the method of determination of the liquid compositions. Kushiro *et al.* (1972), Kushiro

(1973a, b), Mysen and Boettcher (1975) and Mysen and Kushiro (1977) reported EPMA (Electron Probe X-ray Micro-Analyzer) analyses of quenched glasses as representing equilibrium liquid compositions. Green (1973) and Jaques and Green (1979, 1980), on the other hand, pointed out that the glass compositions are significantly modified by overgrowth of adjacent solids during quenching. They estimated equilibrium liquid compositions by mass balance calculations based on compositions and modal amounts of solid residues. However, estimation by this method also includes considerable uncertainties because of compositional zoning in minerals and uncertainties in the estimation of their modal amounts.

In this paper we present new experimental results on the anhydrous melting of a spinel lherzolite from Salt

Lake Crater, Hawaii (HK66101703, designated HK66 hereafter). The melting behavior of the rock was originally studied by Kushiro *et al.* (1968) both under dry and wet conditions. In order to overcome the quench modification of liquid compositions, a special experimental technique was employed in the present experiments, whereby a thin layer of basalt powder is sandwiched between compressed peridotite minerals and then is equilibrated with its host at melting temperatures (basalt/peridotite sandwich technique, see Fig. 3). This technique is essentially the same as the mineral capsule technique developed by Walker *et al.* (1979) for one atmosphere experiments and which has been used by Stolper (1980) and Takahashi (1980a, c) at high pressures. Melt compositions formed near the solidus of HK66 were determined with the above technique.

It was concluded that most of the previously reported direct EPMA glass analyses are in error judging from the Fe–Mg partition coefficient between olivine and liquid obtained in our experiments. A general set of isobaric liquid compositional trends for peridotite partial melting under dry conditions was obtained in CIPW normative projections, and the origin of mid-ocean ridge basalts was discussed on the basis of the liquid compositional trend.

Difficulties of peridotite melting experiments

There are at least three major difficulties in conducting melting experiments of natural peridotite at high pressures and determining equilibrium liquid compositions. They are (1) inevitable chemical reactions between the peridotite partial melt and the container, (2) modification of the partial melt compositions during quenching, (3) slow reaction rate of residual solids with melt.

Capsule materials

Noble metals such as Pt and Ag–Pd alloy have been used most frequently as capsule materials in peridotite melting experiments (*e.g.*, Mysen and Boettcher, 1975; Jaques and Green, 1980). It is well known, however, that Fe and Ni alloy with those noble metals at high temperatures, which results in strong compositional zoning in solids (*e.g.*, Jaques and Green, 1980, p. 289). Upon formation of the alloy, excess oxygen is produced and part of the FeO in the melt is oxidized to $\text{FeO}_{1.5}$ (*e.g.*, Yoder and Tilley, 1962, p. 391). At 1400°C and 20 kbar, the mole ratio $\text{FeO}_{1.5}/\text{FeO}$ of a basalt melt embedded in Fo_{90} olivine in sealed Pt capsule was found to have changed from 0.12 (1 hr) to 0.50 (48 hr) (Takahashi, 1980a). Thus, oxygen fugacities of the charges in the noble metal capsules change as a function of run duration and are more oxidizing than previously expected.

Graphite was found to be the most suitable capsule material for the present experiments for the following reasons. According to Thompson and Kushiro (1972), the oxygen fugacity of the experimental charge in a graphite capsule is within the stability field of wüstite in the

pressure range between 10 and 20 kbar, and temperatures between 1200° and 1500°C. Precipitation of nickel metal exsolved from olivine was observed by the present authors in the melting experiments of peridotite at all pressures and temperatures. However, the amount of iron alloying with the nickel metal becomes significant only at pressures less than 10 kbar, hence the $\text{Mg}/(\text{Mg} + \text{Fe})$ ratios of solids were constant as a function of run durations at least up to 60 hr.

It is of considerable importance that the amount of Fe^{3+} in a basalt melt is negligibly small in a graphite capsule (less than the detection limit of ^{57}Fe Mössbauer spectroscopy in a number of basaltic glasses; that is less than about 5% of total iron: Takahashi, unpublished data). Therefore, the Fe^{2+} –Mg partition coefficient between coexisting melt and solids can readily be calculated from the EPMA analyses.

Quench problem

Results of line traverse analyses of olivine and adjacent quenched liquids are shown in Figure 1. The compositions of the glass quenched at 15 kbar (Fig. 1B) are significantly modified at the contact with olivine. Because the run product was quenched after a long run duration (61 hr), it is not likely that the zoning represents a growth effect of the olivine throughout the run time. Alternatively, the zoning is considered to have been formed by overgrowth of the olivine during quenching (quenching rate: 200°C/sec to 400°C/sec). The quench modification of the partial melt is more serious as temperature and pressure increase because the melt becomes more picritic at high pressures and temperatures. The extent of the zoning in the quenched liquid also depends on the volume proportion of the liquid to solids (the smaller the amount of liquid the greater the extent of zoning). The partial melt is virtually unquenchable at pressures above about 30 kbar where acicular or dendritic quench crystals are formed instead of quench glass (Fig. 1A). Similar observations have been made by Kushiro (1974).

Jaques and Green (1979) focussed on this problem in more detail and concluded that equilibrium composition of the peridotite partial melt can not be determined by direct EPMA analysis of the quenched glass at any pressure and temperature conditions. Accordingly, they estimated equilibrium liquid compositions by mass balance calculations. Precision of such calculations, however, may not be sufficient because small error in the estimation of modal proportion significantly affects compositions of small amounts of melts (Mysen and Boettcher, 1975, p. 576–578). In addition, the chemically zoned crystals in their charges (Jaques and Green, 1980, p. 294–298) made it impossible to evaluate standard errors in their estimation. Therefore, the special experimental technique (basalt/peridotite sandwich technique) was employed by the present authors. Because the glass disk inserted between two peridotite layers (Fig. 3) contains a very small amount of crystals, the quench overgrowth

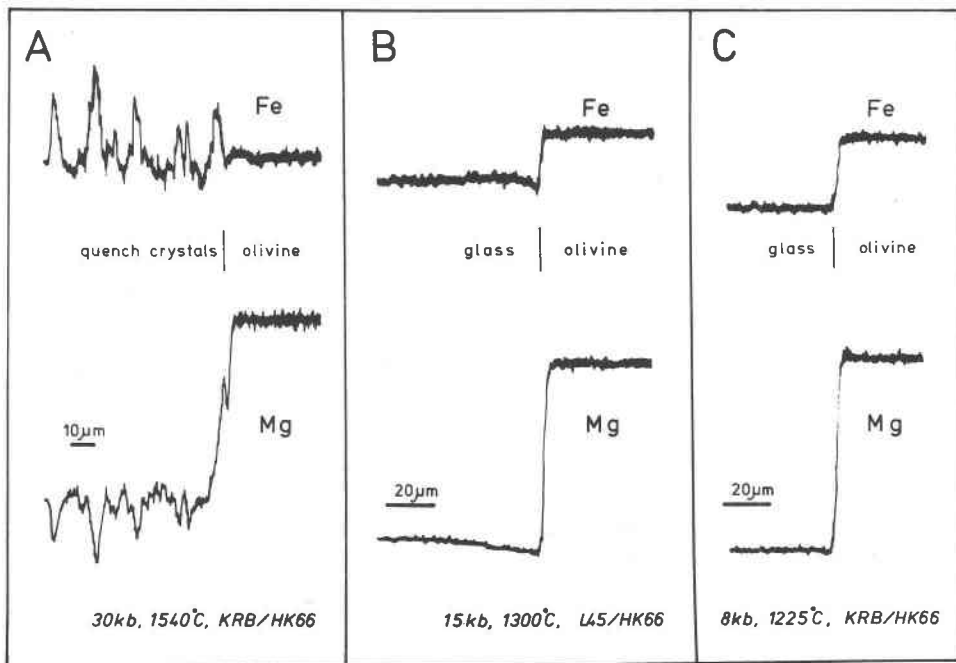


Fig. 1. Line traverse analysis of olivines and adjacent quenched liquids obtained at basalt melt-peridotite boundaries using the basalt/peridotite sandwich technique (*cf.*, Fig. 3). The effect of crystal overgrowth during quenching on compositions of adjacent liquids becomes serious as pressure increases. The glass in Fig. 1B shows a variation in MgO from 11.0 wt.% (left) to 7.0 wt.% (contact). (A, Run #48; B, Run #40; C, Run #30).

effect of solids on liquid compositions was limited only to the boundaries with the peridotite (Fig. 1). Liquid compositions equilibrated with the peridotite were determined with EPMA by analyzing the center of the glass disk.

Slow reaction rates in solids

This problem has been considered very little by previous workers. In Figure 2, an example of relict pyroxene crystals is shown after a run at 8 kbar and 1200°C for 40 hr. The orthopyroxene retains the composition of the starting material in the core and is surrounded by newly formed alumina-poor orthopyroxene in the rim. At the boundary between the two pyroxenes, the Ca and Al contents show an abrupt change, indicating that those elements were not transferred through the boundary. The Fe and Mg, on the other hand, appear to have exchanged to some extent, judging from the zoning pattern.

Interpretation of the above observation is as follows. Upon melting of a peridotite whose mineral compositions inherit equilibration at different pressure-temperature conditions (this is always the case in experimental peridotite melting), melting is initiated by melting of the metastable solids. Chemical reaction between the residues and the partial melt takes place subsequently, but the rate of the reaction is limited by the diffusion process in the solids, so that the relict compositions remain for a long time. The run durations of our experiments were intended to be as long as possible. Achievement of chemical

equilibrium of the run products was examined by time studies and extensive chemical analyses with EPMA such as those by Takahashi (1980b).

Experimental and analytical procedures

Most of the experiments were made with three piston-cylinder apparatus at the Geophysical Laboratory, Carnegie Institution of Washington (Boyd and England, 1960). Some of them were made with a piston-cylinder at Tokyo University. The piston-out technique was employed. The ½ inch diameter, talc-pyrex assembly was used with a graphite heater and sintered alumina as an inner spacer. In order to run more than two charges simultaneously, the ¾ inch diameter assembly with a tapered graphite heater and sintered MgO spacer (Kushiro, 1976) was used for some runs at pressures less than 20 kbar.

Temperatures were measured with Pt/Pt₉₀-Rh₁₀ thermocouples in runs below 1450°C. At higher temperatures, W₉₅-Re₅/W₇₅-Re₂₅ thermocouples were used. The two thermocouples were calibrated against each other at a low oxygen fugacity in a one-atmosphere furnace. The uncertainty in their comparison is less than 2°C at 1400–1500°C. No pressure correction was made on the emf of the thermocouple. Run temperatures were controlled to within ±3°C with a silicon-controlled rectifier. Due to the thermal gradient in the furnace assembly, however, uncertainties in temperature measurements may be greater

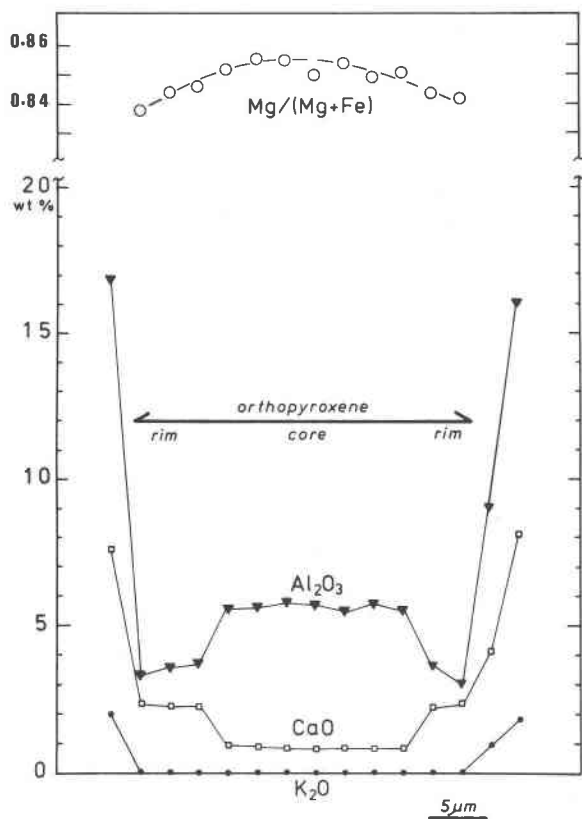


Fig. 2. Line traverse analysis of an orthopyroxene with a relict crystal in the core (Run #28, KRB/HK66). See Table 4 for full chemical analysis of the core and the rim.

than 10°C in runs with the ½ inch assembly. In runs with the ¾ inch tapered furnace assembly, however, temperature variation among the charges run simultaneously is believed to be less than 10°C (Kushiro, 1976).

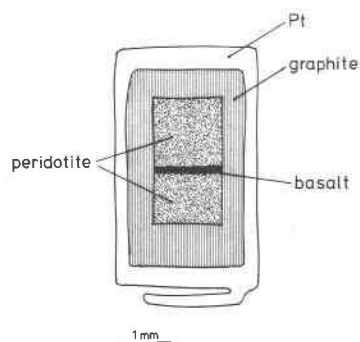


Fig. 3. A schematic illustration showing cross section of the experimental charge used in order to determine equilibrium liquid compositions (Runs #26-51, 60-64). A thin layer of powdered basalt is sandwiched between compressed blocks of powdered peridotite minerals.

In experiments for solidus determination (Runs #1-25), a 10 mg charge of powdered peridotite (average grain size less than 10 μm; see Table 1 for chemical composition) was encased in a graphite capsule (2.5 mm O.D.), which was then sealed in a Pt-capsule (3 mm O.D.). In experiments for liquid composition determination (Run #26-51), a 1 mg disk of basalt powder (less than 10 μm in grain size, see Table 1 for chemical compositions) was embedded in about 10 mg of the peridotite powder which was then encased in the above double capsule (Fig. 3). The basalt powder melted at the beginning of the experiments and subsequently mixed with the partial melt formed along the grain boundaries in the peridotite matrix. In experiments along the solidus, the basalt melt stayed in its original position and was quenched as a coherent glass disk (300-500 μm in thickness) even after more than several days. At temperatures more than 100°C above the solidus, however, the basalt melt tends to disperse in the peridotite matrix. On the other hand, segregation of the

Table 1. Compositions of the starting materials

	Peridotite HK66					Basalts				
	bulk†	ol*	opx*	cpx*	sp*	KRB††	L45††	K21††	OCE††	BON**
SiO ₂	48.02	38.76	53.50	50.93	0.12	47.8	49.5	49.9	46.0	57.6
TiO ₂	0.22	0.00	0.11	0.55	0.21	2.4	1.7	2.9	2.0	0.3
Al ₂ O ₃	4.88	0.00	5.27	7.35	61.31	17.3	15.1	12.9	8.2	15.8
FeO ^o	9.90	14.41	8.71	4.30	15.34	9.3	11.4	11.2	13.4	7.2
MnO	0.14	0.17	0.13	0.09	0.13	0.2	0.2	0.2	0.2	0.2
MgO	32.35	45.89	31.13	14.62	19.53	8.8	8.5	9.2	21.0	8.5
CaO	2.97	0.07	0.71	18.75	0.04	8.1	10.6	11.0	7.2	7.8
Na ₂ O	0.66	0.00	0.13	1.96	0.00	3.7	2.7	2.2	1.7	1.9
K ₂ O	0.07	n.d.	n.d.	n.d.	n.d.	1.7	0.1	0.5	0.3	0.7
P ₂ O ₅	0.07	n.d.	n.d.	n.d.	n.d.	0.7	0.?	n.d.	n.d.	n.d.
Cr ₂ O ₃	0.25	0.00	0.16	0.50	2.66	n.d.	n.d.	n.d.	n.d.	n.d.
NiO	n.d.	0.35	n.d.	n.d.	0.45	n.d.	n.d.	n.d.	n.d.	n.d.
Total	99.53	99.65	99.85	99.05	99.79	100.0	100.0	100.0	100.0	100.0

*, EPMA analysis (this study); †, Kushiro et al. (1968); ††, Takahashi (1978); **, Shiraki and Kuroda (1977).

partial melt (mixed with the embedded basalt melt) from residual solids was observed in those high temperature runs.

To drive out moisture from the charge, all the starting materials were dried at 1100°C and QFM buffer in a one-atmosphere quenching furnace using the method of Pressnall and Brenner (1974) in order to minimize iron-loss, and then were quenched on a cold metal plate in a reduced gas mixture of CO and CO₂. The sample assembly was stored in an oven at 110°C immediately prior to welding the Pt capsule.

After they were quenched at high pressures, the charges were sectioned parallel to the length of the furnace assembly, and phases were identified with a reflected light microscope. Run products of subsolidus conditions were examined also with the X-ray diffractometer. Chemical analyses were made with an automated electron microprobe at the Geophysical Laboratory with a specimen current of 0.02 μ A, 2–3 μ m beam diameter, and 20–40 seconds counting time for each element. Additional chemical analyses were made with an electron microprobe (JXA-5A) at the Institute for Thermal Spring Research. For the glass analyses, a large defocussed electron beam (30–50 μ m diameter) was employed in order to avoid volatilization of alkalis during the analysis. The analyses of the glasses show no systematic deficiency in total (see Table 3), thus it is believed that volatiles (H₂O, CO₂) were not significantly dissolved in the melt.

Chemical equilibrium in the basalt/peridotite sandwich experiment

Ranges of cationic diffusion coefficients in minerals and melt relevant to the present experiments are summarized in Figure 4. Characteristic diffusion distances ($X = \sqrt{Dt}$, where D represents a cation diffusion coefficient and t is a run duration) are shown as a function of run duration. The times required for solids to achieve chemical equilibrium by diffusion were calculated on the basis of a simple model with a spherical boundary condition ($t = 0.4 (r^2/D)$, where r denotes radius of a sphere, Crank, 1956, Fig. 6-1). The typical grain size of residual solids in the quenched charges is 10–20 μ m, hence it is believed that the Fe–Mg exchange equilibrium between olivine and liquid was achieved at least in the long runs. Cores of pyroxene crystals greater than 10 μ m in diameter probably were out of equilibrium even after more than a week if solid diffusion is the reaction process (cf. Fig. 2). Characteristic diffusion distances for basaltic melts are more than 1 mm (Fig. 4), hence, it is likely that homogenization of basalt melt with the partial melt of the peridotite was completed during the first several hours in the basalt/peridotite sandwich experiments (Fig. 3).

To test the above considerations, a time study was made at 15 kbar and 1300°C (Runs #38–40). Charges consisting of different basaltic rocks sandwiched in the peridotite HK66 were run simultaneously in the large

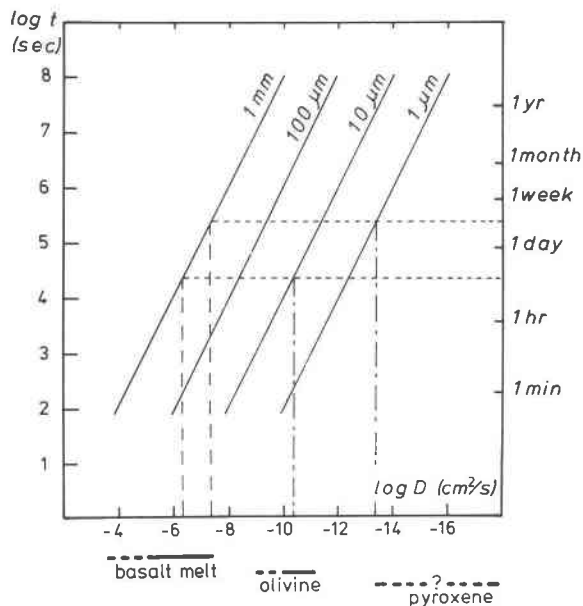


Fig. 4. Time vs. chemical diffusion relationships for the peridotite melting experiments. Diffusion coefficients from the following sources: Na, Ca, Sr, Ba in basalt melts, Hofmann (1980) and Watson and Bender (1980); Fe–Mg in olivine, Misener (1974); Ni, Mn, Ca and Mg in olivine, Morioka (1981); Ca–Mg in pyroxenes, Takahashi (1980b) and McCallister (1980). Solid lines are diffusion distances (\sqrt{Dt}) as a function of run duration and diffusion coefficient. Broken lines indicate approximate ranges for the present experiments.

capacity $\frac{3}{4}$ inch assembly. Compositions of the basalt melts initially were greatly different (quartz-normative to nepheline-normative), but became very similar after a day and stayed constant for another 1.5 days (Fig. 5). No compositional heterogeneity was observed in the liquid disk except at the boundary between peridotite and melt where quench modification of liquid compositions had taken place (Fig. 1). Similarities of the final liquid compositions are well illustrated in a CIPW normative plot (Fig. 6), where compositions of the starting materials are shown for comparison. Also shown in the figure are compositions of liquids equilibrated with the peridotite at another pressure and temperature (8 kbar and 1225°C).

The fact that liquids initially formed from various starting materials converged to very similar compositions indicates at least two things: (1) homogenization of the partial melt in peridotite and the embedded basalt melt was completed within a day; and (2) compositions of melts coexisting with the olivine + orthopyroxene + clinopyroxene buffer at given pressure–temperature conditions have only limited ranges of variation.

Minor but important differences in K₂O and SiO₂ are seen among the liquid compositions. The liquids which were initially alkali-olivine basalt (KRB) show higher K₂O and SiO₂ contents than liquids which were other basalt compositions (Table 3, Fig. 5). The difference in K₂O

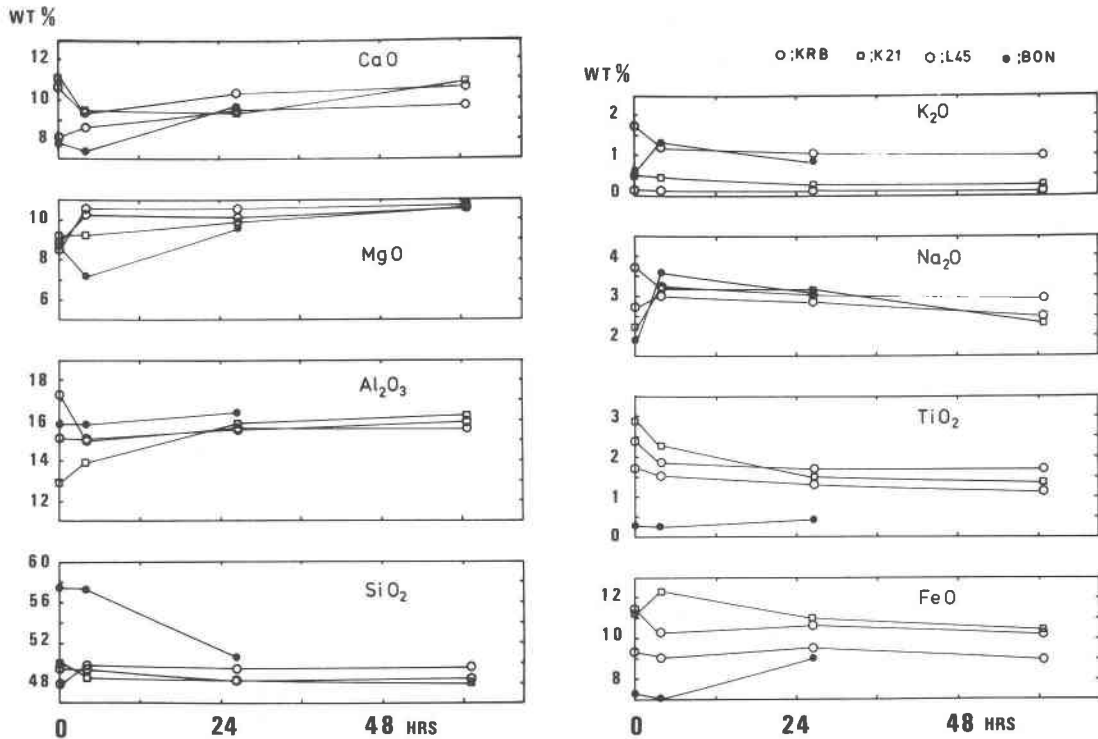


Fig. 5. Compositions of melts sandwiched between partially molten peridotite as a function of time at 15 kbar and 1300°C (Runs #38–40). Regardless of the starting basalts, the melts are almost identical after one day and remain constant for another 1.5 days.

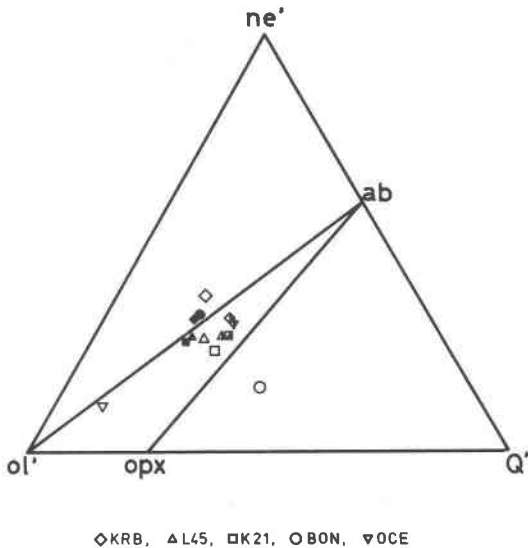


Fig. 6. Normative compositions of the basalt starting materials listed in Table 1 (open symbols); melts equilibrated with the peridotite at 8 kbar and 1225°C (half solid symbols); and those at 15 kbar and 1300°C (solid symbols). Regardless of the starting materials, melts equilibrated with the peridotite at a given pressure–temperature condition show similar normative compositions. After projection scheme described by Irvine and Baragar (1971) based on cation mole percent norms.

is considered to be a signature of the starting material, inasmuch as the peridotite is virtually potassium free. Because there are no peridotite constituent minerals that incorporate this element in solid-solution, K_2O in the melt can not be buffered but depends only on the volume proportion of the liquid in the charge. Observed increase in SiO_2 with K_2O accords with the expected shift of the olivine–orthopyroxene liquidus boundary noted by Kushiro (1975). Thus, minor differences among the liquid compositions at a given pressure–temperature condition reflect the complex variation of chemical equilibria in a multi-component system.

The compositions of solid phases formed during the time studies were examined with EPMA. Cores and rims of three or more crystals in the glass disk were analyzed for each mineral. The minerals in the peridotite matrix were analyzed with a grid-mode automated stage motion (3 or 5 μm interval) for more than 200 points in each sample. The latter data included some analyses in which the beam overlapped more than two minerals and/or liquid. Data characterized by abnormal stoichiometry or high K_2O content were discarded.

The $Mg/(Mg + Fe)$ ratio of olivine shows a bimodal distribution in short runs because of the higher $Mg/(Mg + Fe)$ ratio of the embedded basalts compared with the peridotite (see Table 1). The $Mg/(Mg + Fe)$ of olivine in

long runs, however, is limited to a narrow range and there is no difference between the olivine in the liquid disk and that in the peridotite matrix (Fig. 7). The Ca content of pyroxenes, on the other hand, shows a large variation even in long runs. A large number of relict pyroxenes (both orthopyroxene and clinopyroxene) were found in the runs particularly at lower pressures (Fig. 2). It should be emphasized that the occurrence of the pyroxene relicts is not limited to the basalt/peridotite sandwich experiments but is common in peridotite melting experiments at relatively low pressure and temperature conditions.

Tsuchiyama and Takahashi (in press) have studied kinetics of partial melting of a plagioclase feldspar (An₆₀) at one atmosphere under dry conditions. According to them, the melting process is rate-controlled by chemical diffusion in the plagioclase and it took several hundred hours even at 1400°C before the solid achieved final chemical equilibrium with the partial melt. Nevertheless, surface chemical equilibrium between the partial melt and the residue was established and the chemical composition of the melt, which is identical to the equilibrium liquid composition determined by Bowen (1913), was unchanged during the experiment. It is unlikely, therefore, that the liquid compositions are largely out of equilibrium in the peridotite melting experiments even in the charges with a great amount of relict crystals.

In summary, it is shown that chemical equilibrium between the melt (including the basalt melt and the peridotite partial melt) and olivine is achieved throughout the experimental charges at least in the runs more than a day long. Only the rims of pyroxenes are likely to have compositions in equilibrium with the melt. Core compositions of the pyroxenes are nearly isolated from the system and react slowly.

Solidus

The solidus of the peridotite HK66 was originally studied by Kushiro *et al.* (1968) with a tetrahedral-anvil type, solid-media high pressure apparatus, but there were large uncertainties in the pressure calibration below 30 kbar (Akimoto, personal communication, 1980). Furthermore, the uncertainty in temperatures may be of the order of 100°C because of a steep thermal gradient in the small furnace assembly used in the previous work (Takahashi *et al.*, 1982). The solidus, therefore, was redetermined in the present study with a piston-cylinder apparatus (Runs #1–25, Fig. 8). One-atmosphere experiments (Runs #1–5) were carried out under controlled oxygen fugacity (QFM) using the Pt-loop method of Presnall and Brenner (1974) with crystalline starting material that had been annealed at 15 kbar and 1200°C for 2 hr.

The revised solidus is generally at temperatures 70–100°C lower than the original curve. This difference may be partly due to the large uncertainties in experimental pressures and temperatures in the previous study, but also reflects the difference in technique in identifying run

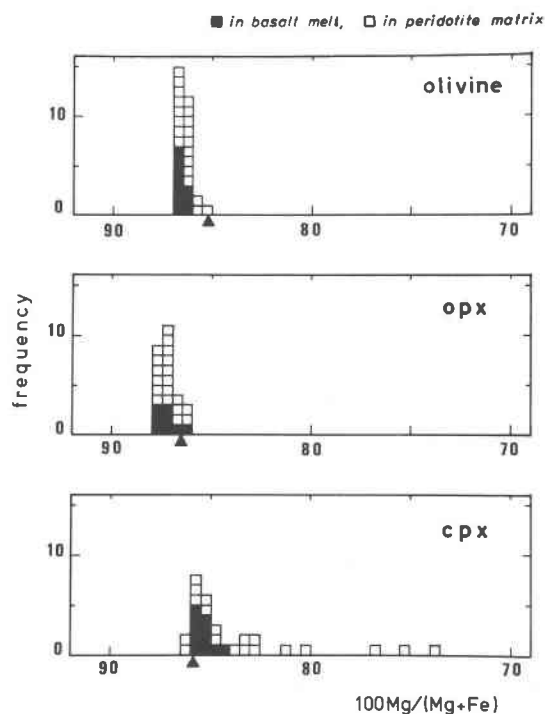


Fig. 7. The Mg-values of olivine and pyroxenes in an experimental charge quenched after 61 hr at 15 kbar and 1300°C (Run #40, L45/HK66). Crystals in the liquid domain (see Fig. 3) are distinguished by solid squares, those in peridotite matrix by open squares. The inverted triangles indicate compositions of starting materials. Clinopyroxenes rich in Fe are quench crystals.

products. Under the reflected light microscope, which has been used in the present study instead of the transmitted light microscope of the previous study, glass quenched from partial melt is readily identified even in small amounts, and even quench crystals are distinct in that they characteristically show dendritic shapes. Chemical analyses and back-scattered X-ray images of the run products by EPMA were useful in identifying the two pyroxenes and isolating plagioclase from quenched liquid (see Table 2 for mineral assemblages of the run products).

It should be noted that no spinel was observed in the experiments above 15 kbar, although it was reported by Kushiro *et al.* (1968) and would be easily identified in polished sections because of its high reflectivity and characteristic equant shape. There are two possible reasons for its absence: (1) with long run durations in the present study, all the Al₂O₃ in the spinel dissolved either in the melt or in pyroxenes; (2) because of the low oxygen fugacity imposed by the graphite capsule, Cr³⁺ that stabilizes spinel greatly (*e.g.*, Irvine, 1977) was reduced to Cr²⁺ which then dissolved in olivine and pyroxenes (note higher chromium content of olivine in Table 4, also contrasting results with Fe and Pt containers by Jaques and Green, 1980). The subsolidus mineral assemblage of

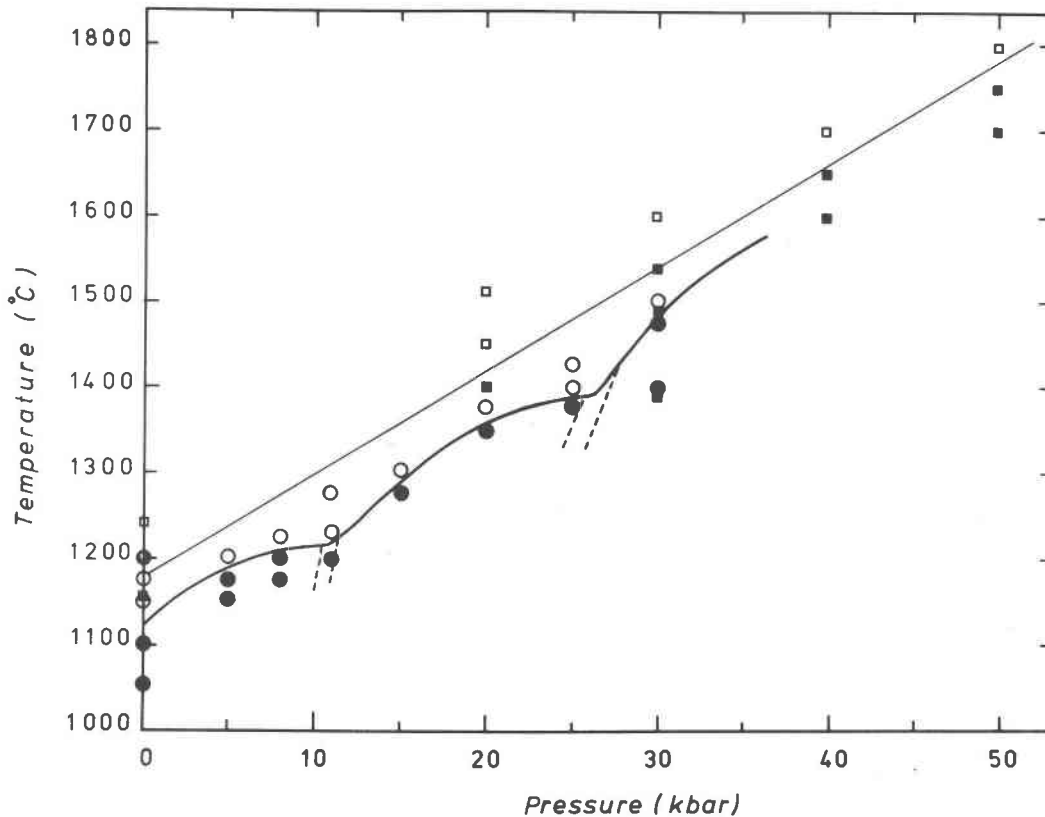


Fig. 8. Solidus curve of the peridotite HK66 under dry conditions (circles and solid lines) have cusps at about 11 kbar and 26 kbar where subsolidus mineral assemblage changes from plagioclase lherzolite to aluminous pyroxene lherzolite, and aluminous pyroxene lherzolite to garnet lherzolite, respectively. Data of previous study (Kushiro *et al.*, 1968) are given for comparison (squares and light line). Solid symbols denote subsolidus runs and open symbols with quenched liquid.

HK66 between 10 and 25 kbar corresponds to the aluminous pyroxene peridotite of Green and Ringwood (1967b).

Additional experiments were made with garnet seeds (3 wt.% of pyrope-rich garnet) in the peridotite (Runs #20 and 23). The amount of garnet increased in the run at 30 kbar, whereas it diminished at 25 kbar. Thus, garnet is considered to be a stable subsolidus phase above a pressure between 25 and 30 kbar, although it was not nucleated in some experiments (see Table 2).

Finally it is noted that the solidus determined in the present experiments is not satisfactorily fitted with a straight line. It agrees, however, with the observation by Presnall *et al.* (1979) and Presnall and Hoover (1982) that the solidi for simplified peridotite systems have cusps at points where the subsolidus phase assemblage changes. As shown in Figure 8, the present results can be interpreted as representing three curves defining cusps at transitions from plagioclase lherzolite to aluminous-pyroxene lherzolite at about 11 kbar and from aluminous-pyroxene lherzolite to garnet lherzolite at about 26 kbar.

Compositions of melts and solids along the solidus

The compositions of the melts formed at temperatures just above the dry solidus of HK66 were determined with the basalt/peridotite sandwich technique (Table 3). The melt compositions formed at higher temperatures are also listed in the same table. Selected analyses of coexisting solid phases are given in Table 4.

At 5 kbar, the melt near the solidus, which coexists with olivine, orthopyroxene and clinopyroxene is a quartz tholeiite. At 8 kbar, the near solidus melt is an olivine tholeiite. At 10 kbar, it is also olivine tholeiite, but is slightly enriched in MgO and Na₂O and depleted in SiO₂ compared to that at 8 kbar. At 15 and 20 kbar, the melts are nepheline normative alkali-olivine basalt richer in alkalis and poorer in SiO₂ than the liquids at 8 and 10 kbar. At 25, 30 and 35 kbar, they are picritic melts characterized by high MgO contents.

Because the degree of partial melting increases abruptly in this pressure range (Mysen and Kushiro, 1977), clinopyroxene was absent in residues in all runs above 25

Table 2. Run details

Run #	P (kbar)	T (°C)	Dura- tion (hr)	No. of charges	Starting materials		Assemblages*
					peridotite	basaltic components	
1	0.001	1050	13.0	1	HK66+		ol, opx, cpx, sp, pl
2	0.001	1100	17.0	1	HK66+		ol, opx, cpx, sp, pl
3	0.001	1150	23.5	1	HK66+		ol, opx, cpx, L
4	0.001	1175	14.5	1	HK66+		ol, opx, cpx, L
5	0.001	1200	3.0	1	HK66+		ol, opx, L
6	5	1150	17.5	1	HK66		ol, opx, cpx, sp, pl, m
7	5	1175	2.0	1	HK66		ol, opx, cpx, sp, pl, m
8	5	1200	46.5	1	HK66		ol, opx, cpx, sp, pl, m, L
9	8	1175	2.0	1	HK66		ol, opx, cpx, sp, pl, m
10	8	1200	1.3	1	HK66		ol, opx, cpx, sp, pl, m
11	8	1225	41.0	1	HK66		ol, opx, cpx, sp, m, L
12	11	1200	4.0	1	HK66		ol, opx, cpx, sp, m
13	11	1230	2.0	1	HK66		ol, opx, cpx, sp, L
14	11	1275	2.0	1	HK66		ol, opx, cpx, L
15	15	1275	72.0	1	HK66		ol, opx, cpx, sp, m, L?
16	15	1300	61.0	1	HK66		ol, opx, cpx, m, L
17	20	1350	45.0	1	HK66		ol, opx, cpx, m
18	20	1375	23.5	1	HK66		ol, opx, cpx, m, L
19	25	1375	6.0	1	HK66		ol, opx, cpx, sp, m
20	25	1375	2.5	1	HK66 ^o		ol, opx, cpx, sp
21	25	1400	1.8	1	HK66		ol, opx, cpx, m, L
22	25	1425	2.0	1	HK66		ol, opx, cpx, L
23	30	1400	1.5	1	HK66 ^o		ol, opx, cpx, gt, sp
24	30	1475	4.5	1	HK66		ol, opx, cpx
25	30	1500	3.0	1	HK66		ol, opx, cpx, L
26	5	1200	46.5	2	HK66	*KRB, L45	ol, opx, cpx, sp, pl, m, L
27	5	1225	10.5	2	HK66	*KRB, L45	ol, opx, cpx, m, L
28	8	1200	40.0	2	HK66	*KRB, L45	ol, opx, cpx, sp, pl, m, L
29	8	1225	29.0	2	HK66	*L45, K21	ol, opx, cpx, sp, m, L
30	8	1225	41.0	3	HK66	*KRB, OCE, BON	ol, opx, cpx, sp, m, L
31	8	1250	19.0	2	HK66	*L45, K21, L	ol, opx, m, L
32	8	1275	4.0	2	HK66	*L45, K21	ol, opx, m, L
33	8	1275	14.0	2	HK66	*L45, K21	ol, opx, m, L
34	10	1250	26.0	2	HK66	*L45, K21	ol, opx, cpx, m, L
35	10	1275	25.0	2	HK66	*L45, K21	ol, opx, cpx, L
36	10.5	1290	30.0	3	HK66	*L45, KRB, OCE	ol, opx, L
37	15	1275	72.0	3	HK66	*KRB, L45, K21	ol, opx, pig, cpx, m, L
38	15	1300	4.0	4	HK66	*KRB, L45, K21, BON	ol, opx, cpx, sp, m, L
39	15	1300	26.5	4	HK66	*KRB, L45, K21, BON	ol, opx, pig, cpx, m, L
40	15	1300	61.0	4	HK66	*KRB, L45, K21, BON	ol, opx, pig, cpx, m, L
41	15	1350	23.5	1	HK66	KRB	ol, opx, L
42	15	1400	36.0	2	HK66	*KRB, L45	ol, opx, L
43	20	1375	23.5	2	HK66	*KRB, L45	ol, opx, cpx, L
44	20	1400	48.0	1	HK66	KRB	ol, opx, L
45	25	1425	16.5	1	HK66	KRB	ol, opx, m, L
46	25	1450	14.5	1	HK66	KRB	ol, opx, m, L
47	30	1520	19.0	1	HK66	KRB	ol, opx, m, L
48	30	1540	8.5	1	HK66	KRB	ol, opx, m, L
49	30	1550	4.5	1	HK66	KRB	ol, opx, m, L
50	30	1550	12.5	1	HK66	L45	ol, opx, m, L
51	35	1600	2.5	1	HK66	KRB	ol, opx, m, L

kbar even at temperatures closest to the solidus. Because pyroxenes in the peridotite matrix frequently show relict compositions (Fig. 2) and the effect of quench crystallization on composition of solids is more conspicuous in the peridotite matrix than in the liquid disk (Fig. 7), analyses of coexisting solids within the liquid disk of the charges were adopted (Table 4). It is notable that pigeonitic clinopyroxene coexists with orthopyroxene and subcalcic augite at 15 kbar. According to Lindsley (1980), the lower stability of pigeonite in the quadrilateral pyroxene system is about 1350°C at 15 kbar and $Mg/(Mg+Fe) = 0.85$. The present observation suggests that the limit actually is more than 50°C lower in the presence of other components (*e.g.*, Al_2O_3).

Effect of K_2O on the solidus and the melt compositions

Because K_2O is incompatible in all anhydrous peridotite minerals, it is likely that K_2O plays a role analogous to that of volatiles in the melting of a dry peridotite. In their study of the system $K_2O-MgO-Al_2O_3-SiO_2$ (KMAS) at high pressures, Wendlandt and Eggler (1980) showed that the solidus of a simplified K_2O -bearing peridotite involves the following reactions: $Sa + En = Fo + L$ (6–18 kbar); $Sa + Fo + En = L$ (18–19 kbar); $Sa + Fo = En + L$ (19–34 kbar); and $Ks + En = Fo + L$ (above 34 kbar); where Sa, Fo, En, Ks and L denote sanidine, forsterite, enstatite, kalsilite and liquid, respectively.

Table 2. (continued)

Run #	P (kbar)	T (°C)	duration (hr)	No. of charges	Starting materials		Assemblages
					peridotite	basaltic components	
52	20	1250	4.5	1	HK66'		ol, opx, cpx, sp, sa
53	20	1300	3.5	1	HK66'		ol, opx, sp, L
54	20	1330	2.5	1	HK66'		ol, opx, L
55	30	1300	2.0	1	HK66'		ol, opx, cpx, sp, gt?, sa
56	30	1350	1.0	1	HK66'		ol, opx, sp, L
57	30	1400	2.5	1	HK66'		ol, opx, L
58	37	1300	2.5	1	HK66'		ol, opx, cpx, sp, gt, sa
59	37	1350	2.0	1	HK66'		ol, opx, gt, L
60	20	1300	4.5	1	HK66''	KFSB-1	ol, opx, cpx, sp, L
61	20	1330	2.5	1	HK66''	KFSB-1	ol, opx, L
62	30	1400	6.0	1	HK66''	KFSB-1	ol, opx, cpx, sp, sa, L
63	30	1450	2.0	1	HK66''	KFSB-2	ol, opx, cpx, L
64	30	1475	4.0	1	HK66''	KFSB-3	ol, opx, cpx, L

* , for runs with more than one charges, phase assemblage of a representative charge is given;
HK66', preannealed at 15 kbar and 1200°C; HK66°, seeded with pyrope-rich garnet.

HK66', HK66 plus 20 wt % of adularia; HK66'', HK66 plus 2 wt % of adularia;
KFSB-1, KRB plus 50 wt % of adularia; KFSB-2, KRB plus 20 wt % of adularia;
KFSB-3, KRB plus 10 wt % of adularia.

abbreviations; ol, olivine; opx, orthopyroxene; pig, pigeonite; cpx, Ca-rich clinopyroxene;
sp, spinel; pl, plagioclase; gt, garnet; m, Fe-Ni metal; sa, sanidine; L, liquid.

An attempt has been made to examine the anhydrous reactions in a K₂O-rich natural peridotite, using the peridotite HK66 plus 20 wt.% adularia as a starting material (Runs #52-59). Sanidine was observed in the subsolidus runs at least up to 37 kbar and the solidus was lowered by about 100°C relative to that in the KMAS

system (cf., Fig. 9 with Fig. 13 of Wendlandt and Egger, 1980). This difference is reasonable in view of the FeO content of olivine and pyroxenes, but it may also be possible that clinopyroxene is involved in the reaction in the natural peridotite. Compared with the solidus curve determined with HK66 (Fig. 8), the solidus of the potassic

Table 3. Compositions of the liquids equilibrated with the peridotite

Run #	26	27	30	29	29	30	31	31	33	33	34	34	35	35	36	36	36	37	40	40
P (kbar)	5	5	8	8	8	8	8	8	8	8	10	10	10	10	10.5	10.5	10.5	15	15	15
T (°C)	1200	1225	1225	1225	1225	1225	1250	1250	1275	1275	1250	1250	1275	1275	1290	1290	1290	1275	1300	1300
Compo.*	KRB	KRB	KRB	L45	K21	OCE	L45	K21	L45	K21	L45	K21	L45	K21	KRB	L45	OCE	KRB	KRB	L45
SiO ₂	54.94	54.40	50.91	49.75	50.02	50.38	51.74	50.43	50.95	50.48	48.65	49.71	49.52	49.25	50.27	49.72	49.12	49.14	48.52	48.43
TiO ₂	1.91	1.99	1.41	1.33	1.54	1.52	1.07	1.58	1.16	1.70	1.39	1.45	1.30	1.60	1.45	1.29	1.54	1.59	1.66	1.13
Al ₂ O ₃	15.67	16.20	16.16	15.97	15.95	16.02	15.23	14.36	14.30	13.89	16.59	17.03	15.02	14.54	15.37	14.69	15.16	17.48	15.30	15.89
FeO*	7.50	6.64	7.98	8.87	8.93	8.95	9.41	9.63	9.79	10.09	9.88	9.43	9.55	9.82	8.95	9.98	10.00	8.59	9.34	10.34
MnO	0.11	0.03	0.21	0.18	0.12	0.15	0.19	0.18	0.18	0.14	0.21	0.19	0.19	0.18	0.13	0.18	0.14	0.11	0.15	0.21
MgO	7.42	7.91	8.00	9.05	8.91	8.25	9.81	9.63	10.62	10.28	8.70	8.49	9.95	10.26	10.18	10.93	9.64	8.45	9.95	10.86
CaO	9.09	8.78	10.29	10.61	10.80	11.08	10.38	10.80	9.36	9.57	10.07	10.54	10.40	10.84	9.61	10.36	11.34	7.63	9.30	10.71
Na ₂ O	2.90	2.03	2.81	2.49	2.41	2.51	2.34	2.11	2.36	2.22	3.19	2.98	2.78	2.44	2.52	2.39	2.21	4.00	2.98	2.49
K ₂ O	1.17	0.95	0.72	0.16	0.26	0.31	0.08	0.22	0.09	0.25	0.13	0.26	0.10	0.26	0.79	0.12	0.29	1.55	1.03	0.13
F ₂ O ₅	0.39	0.42	0.22	0.04	0.16	0.18	n.d.	n.d.	n.d.	n.d.	0.08	0.17	0.01	0.16	n.d.	n.d.	n.d.	n.d.	n.d.	n.d.
Cr ₂ O ₃	0.05	0.09	0.07	0.08	0.09	0.07	0.08	0.09	0.10	0.11	0.08	0.09	0.07	0.07	0.05	0.06	0.06	0.04	0.09	0.08
Total	100.15	99.44	98.78	98.53	99.19	99.42	100.33	99.03	98.91	98.73	98.97	100.34	98.89	99.42	99.32	99.72	99.50	98.58	98.32	100.27
CIPW Norm																				
Q	1.76	7.38																		
or	6.90	5.65	4.31	0.96	1.55	1.84	0.47	1.31	0.54	1.50	0.78	1.53	0.60	1.55	4.70	0.71	1.72	9.29	6.19	0.77
ab	24.50	17.27	24.07	21.38	20.56	21.36	19.73	18.03	20.19	19.03	27.27	25.13	23.79	20.77	21.47	20.28	18.79	24.67	23.04	21.02
an	26.24	32.47	29.72	32.40	32.20	31.71	30.71	29.35	28.47	27.55	30.88	32.21	28.53	28.12	28.49	29.08	30.74	25.53	25.76	31.71
ne																		5.23	1.41	
lc																				
di	13.21	6.93	16.72	16.92	16.93	18.30	16.81	20.19	15.05	16.73	15.62	15.38	19.22	20.30	15.85	18.28	21.06	10.49	17.22	17.36
hy	22.79	25.40	13.90	15.82	17.51	16.38	25.40	22.91	26.66	26.15	0.46	5.65	8.36	10.17	12.01	13.57	10.39			2.73
ol			7.96	9.74	7.81	6.98	4.73	5.06	6.73	5.62	22.02	16.85	16.88	15.57	14.63	15.54	14.26	21.66	23.04	24.17
il	3.62	3.80	2.71	2.56	2.95	2.90	2.03	3.03	2.23	3.27	2.67	2.74	2.50	3.06	2.77	2.46	2.94	3.06	3.21	2.14
ap	0.90	0.98	0.52	0.09	0.37	0.42				0.19	0.39	0.02	0.37							
cm	0.07	0.13	0.10	0.12	0.13	0.10	0.12	0.13	0.15	0.16	0.12	0.13	0.10	0.10	0.10	0.07	0.09	0.06	0.13	0.12
Fo**	85.2	86.8	85.5	85.2	85.4	85.2	85.8	85.2	85.9	85.6	83.2	84.1	85.2	85.2	86.1	85.9	85.8	84.4	86.6	85.8
K _D ***	.305	.323	.304	.316	.306	.286	.308	.309	.317	.306	.303	.318	.324	.323	.326	.319	.284	.326	.294	.311

* , additional basaltic components; **, forsterite mole percent of coexisting olivine
***, olivine/liquid iron-magnesium partition coefficient

Table 3. (continued)

Run #	40	39	41	42	42	43	44	45	46	47	48	49	50	51	60	61	62	63	64
P (kbar)	15	15	15	15	15	20	20	25	25	30	30	30	30	35	20	20	30	30	30
T (°C)	1300	1300	1350	1400	1400	1375	1400	1425	1450	1520	1540	1550	1550	1600	1300	1330	1400	1450	1475
Compo.*	K21	BON	KRB	KRB	L45	KRB	KRB	KRB	KRB	KRB	KRB	KRB	L45	KRB	KFSB	KFSB	KFSB	KFSB	KFSB
SiO ₂	47.51	51.30	49.52	50.15	49.89	47.80	49.72	48.77	49.38	46.50	47.84	47.32	47.50	48.63	54.75	53.39	51.00	49.41	47.37
TiO ₂	1.36	0.46	1.06	0.72	0.81	1.55	1.14	1.66	1.18	1.79	1.10	1.16	1.08	1.00	0.78	0.74	0.85	1.79	2.03
Al ₂ O ₃	16.00	16.55	13.39	12.65	12.98	15.60	13.51	15.32	13.78	12.91	11.85	11.34	11.88	10.30	19.33	17.36	15.39	15.57	14.69
FeO [†]	10.32	9.18	8.61	11.08	10.64	9.91	10.36	8.70	10.41	11.03	10.12	10.64	9.21	11.20	4.36	5.94	7.48	8.44	9.56
MnO	0.12	0.18	0.11	0.19	0.25	0.19	0.11	0.14	0.14	0.16	0.21	0.18	0.21	0.12	0.08	0.10	0.13	0.12	0.14
MgO	10.38	9.76	12.39	14.86	14.30	11.20	14.25	12.18	14.39	16.56	18.47	18.91	18.71	21.41	3.80	6.10	8.95	8.79	9.89
CaO	10.79	9.68	10.70	8.15	8.86	9.71	8.02	8.80	8.34	7.25	8.08	6.19	8.84	6.23	3.34	5.07	4.46	6.02	6.18
Na ₂ O	2.30	3.20	2.20	1.42	1.91	3.33	2.34	3.09	2.20	2.72	1.84	1.88	2.11	1.64	2.57	2.27	2.16	2.99	3.51
K ₂ O	0.25	0.87	0.51	0.23	0.07	1.00	0.63	1.26	0.77	1.23	0.55	0.68	0.09	0.64	10.11	7.73	8.45	4.93	3.93
P ₂ O ₅	n.d.	n.d.	n.d.	n.d.	n.d.	0.31	0.16	0.30	0.21	n.d.	0.07	0.15	n.d.	0.09	n.d.	n.d.	n.d.	0.39	0.53
Cr ₂ O ₃	0.04	0.07	0.10	0.19	0.18	0.04	0.15	0.10	0.18	0.08	0.16	0.19	0.11	0.23	0.05	0.05	0.09	n.d.	0.07
Total	99.07	101.25	98.59	99.64	99.89	100.64	100.39	100.32	100.98	100.23	100.29	98.64	99.74	101.49	99.17	98.75	98.96	98.45	97.90
CIPW Norm																			
Q																			
or	1.49	5.08	3.06	1.36	0.41	5.87	3.71	7.42	4.51	7.25	3.24	4.07	0.53	3.73	60.24	46.26	36.42	29.59	23.72
ab	19.64	26.21	18.88	12.06	16.18	17.19	19.72	21.11	18.43	14.03	15.52	16.13	17.90	13.67	0.22	6.47		10.81	10.46
an	32.90	27.88	25.51	27.56	26.67	24.51	24.40	24.13	25.20	19.34	22.38	20.78	22.74	18.58	11.44	14.53	7.42	14.73	12.99
ne		0.29				5.86		2.68		4.84					11.76	7.03	10.00	8.07	10.77
lc																	11.01		
di	17.24	15.97	22.88	10.55	14.05	17.35	11.48	14.07	11.66	13.34	13.76	7.52	17.01	9.07	4.31	8.92	12.13	10.59	12.03
hy	2.74		8.80	34.60	23.79		14.32		11.75		7.60	13.77	2.76	15.87					
ol	23.32	23.61	18.68	12.21	17.10	25.54	23.63	26.61	25.49	37.70	35.01	34.87	36.85	36.68	10.46	15.29	21.25	21.85	24.74
il	2.61	0.86	2.04	1.37	1.54	2.93	2.16	3.14	2.22	3.39	2.08	2.23	2.06	1.87	1.49	1.42	1.63	3.45	3.94
ap						0.71	0.37	0.69	0.48		0.16	0.35		0.21				0.92	1.25
cm	0.06	0.10	0.15	0.28	0.27	0.06	0.22	0.15	0.26	0.12	0.23	0.28	0.16	0.33	0.07	0.07	0.13		0.11
Fo**	85.6	85.3	88.9	87.6	88.0	85.9	87.6	88.5	88.0	88.7	89.7	89.9	91.0	90.2	85.8	86.5	86.4	85.8	85.4
K _p ***	.303	.325	.322	.338	.326	.331	.346	.326	.335	.343	.377	.356	.357	.373	.258	.285	.335	.306	.314

*, additional basaltic components; **, forsterite mole percent of coexisting olivine; ***, olivine/liquid iron-magnesium partition coefficient

Table 4. Selected mineral compositions

Run #	28						35			40					43			47	
P (kbar)	8						10			15					20			30	
T (°C)	1200						1275			1300					1375			1520	
Compo.	KRB						K21			K21					KRB			KRB	
Phase	ol	opx	opx*	cpx	cpx*	sp	ol	opx	cpx	ol	opx	opx*	plg	cpx	ol	opx	cpx	ol	opx
SiO ₂	38.93	53.30	52.45	49.48	49.21	0.59	38.43	54.19	54.07	39.03	53.00	52.05	50.69	50.67	39.54	54.63	52.70	39.99	53.35
TiO ₂	0.07	0.59	0.14	1.30	1.30	0.45	0.02	0.35	0.32	0.04	0.25	0.14	0.32	0.48	0.02	0.20	0.20	0.02	0.25
Al ₂ O ₃	0.13	3.44	5.68	3.41	7.34	55.57	0.00	3.94	2.96	0.02	3.66	4.96	6.66	7.04	0.02	4.73	5.77	0.20	5.04
FeO [†]	15.87	9.78	9.17	6.42	5.15	12.49	14.57	8.26	7.72	14.05	8.69	8.70	8.04	7.06	14.12	8.59	7.41	10.95	6.70
MnO	0.16	0.15	0.20	0.07	0.07	0.15	0.14	0.17	0.13	0.12	0.11	0.18	0.14	0.13	0.19	0.13	0.08	0.14	0.08
MgO	44.38	29.32	30.72	15.87	14.84	19.18	47.01	30.34	24.80	46.57	30.73	30.70	26.22	21.63	46.95	29.95	24.06	47.94	31.39
CaO	0.34	2.28	0.71	21.15	18.17	0.10	0.33	2.80	10.18	0.35	2.41	0.80	5.41	11.57	0.22	2.02	7.30	0.30	1.73
Na ₂ O	0.00	0.00	0.00	0.25	0.84	0.00	0.00	0.00	0.30	0.00	0.00	0.03	0.18	0.31	0.00	0.14	0.53	0.00	0.18
Cr ₂ O ₃	0.08	0.46	0.17	0.40	0.13	10.75	0.06	0.41	0.23	0.07	0.35	0.36	0.39	0.44	0.07	0.32	0.32	0.15	0.25
NiO	0.10	0.09	0.20	0.01	0.01	0.21	0.01	0.07	0.05	0.03	0.05	0.08	0.00	0.03	0.13	0.00	0.14	0.04	0.00
Total	100.06	99.41	99.44	98.36	97.06	99.49	100.57	100.53	100.75	100.28	99.25	98.00	98.05	99.36	101.26	100.71	98.51	99.73	98.97
O=	4.000	6.000	6.000	6.000	6.000	4.000	4.000	6.000	6.000	4.000	6.000	6.000	6.000	6.000	4.000	6.000	6.000	4.000	6.000
Si	0.983	1.896	1.851	1.862	1.840	0.015	0.962	1.893	1.920	0.976	1.879	1.861	1.831	1.832	0.979	1.899	1.894	0.989	1.875
Ti	0.000	0.016	0.003	0.036	0.036	0.008	0.000	0.009	0.008	0.000	0.006	0.003	0.008	0.013	0.000	0.005	0.005	0.000	0.006
Al	0.003	0.144	0.236	0.150	0.323	1.720	0.000	0.162	0.123	0.000	0.153	0.208	0.283	0.299	0.000	0.193	0.244	0.006	0.209
Fe	0.335	0.290	0.270	0.202	0.160	0.274	0.305	0.241	0.229	0.293	0.257	0.260	0.243	0.213	0.292	0.249	0.222	0.226	0.196
Mn	0.003	0.004	0.005	0.002	0.002	0.003	0.003	0.004	0.003	0.002	0.003	0.005	0.004	0.003	0.003	0.003	0.002	0.003	0.002
Mg	1.672	1.554	1.616	0.890	0.827	0.750	1.755	1.579	1.313	1.736	1.625	1.636	1.412	1.165	1.733	1.551	1.289	1.768	1.644
Ca	0.009	0.086	0.026	0.853	0.727	0.002	0.009	0.104	0.387	0.009	0.090	0.030	0.208	0.447	0.005	0.074	0.280	0.007	0.065
Na	0.000	0.000	0.000	0.018	0.060	0.000	0.000	0.000	0.020	0.000	0.000	0.001	0.013	0.021	0.000	0.009	0.037	0.000	0.012
Cr	0.001	0.012	0.004	0.011	0.003	0.223	0.000	0.010	0.006	0.000	0.009	0.009	0.010	0.011	0.000	0.008	0.008	0.003	0.001
Ni	0.001	0.002	0.005	0.000	0.000	0.003	0.001	0.001	0.001	0.000	0.001	0.002	0.000	0.000	0.002	0.000	0.003	0.001	0.006
∑ cation	3.007	4.004	4.016	4.024	3.982	2.998	3.035	4.003	4.010	3.016	4.023	4.015	4.012	4.004	3.014	3.991	3.984	3.003	4.016
MG**	83.3	84.3	85.7	81.7	83.8	73.2	85.2	86.8	85.1	85.6	86.3	86.2	85.3	84.5	85.5	86.1	85.3	88.7	89.3

*, relict minerals; **, 100Mg/(Mg+Fe)

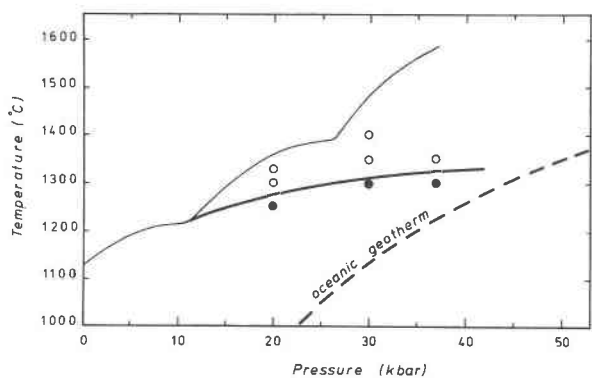


Fig. 9. Solidus curve of the potassic peridotite (circles and bold line) is considerably lower in temperature than the solidus curve defined in Figure 8 (light line). The solidus curve of the potassic peridotite may intersect with the normal oceanic geotherm of Clark and Ringwood (1964) (broken line) at a pressure between 30 and 50 kbar.

peridotite is lowered by about 75°C at 20 kbar and about 150°C at 30 kbar (Fig. 9).

Among constituent minerals in dry peridotite, clinopyroxene is the only phase likely to accommodate potassium. According to Erlank and Kushiro (1970), however, the maximum solubility of K_2O in clinopyroxene is less than 140 ppm. It is likely, therefore, that a trace amount of sanidine is present in the experimental run products of HK66 (which contains 0.07 wt.% K_2O) at pressures above the stability limit of plagioclase under dry subsolidus conditions. The solidus of the potassic peridotite (Fig. 9) should, therefore, be the true dry solidus of HK66.

Throughout the large temperature interval between the two solidi, trace amounts of partial melt could be present (e.g., O'Hara, 1968, Fig. 8), but they would be very difficult to detect. Mysen and Kushiro (1977) found that a trace amount of liquid is present below 1450°C at 20 kbar (where the degree of partial melting increases abruptly) in the melting study of a peridotite PHN1611 containing 0.14 wt.% K_2O . Although they attributed the observation to the presence of moisture in the charge, the same observation was made by one of the present authors (E.T.) with a very well dried starting material of the same rock down to at least 1350°C at 20 kbar. It is thus likely that the existence of such incipient melts below the ordinarily accepted solidus temperature is common in the melting study of natural peridotites under dry conditions.

In order to study the nature of the melt compositions in the temperature interval between the two solidi, a mixture of adularia (50 wt.%) and alkali basalt KRB (50 wt.%) was sandwiched between layers of peridotite HK66 and run at 20 and 30 kbar (Runs #60–64). Trace amounts of the potassium feldspar were also mixed with the peridotite so as to assure the presence of partial melt in the peridotite matrix. Sanidine was present only in the run closest to the solidus (Run #62), but reacted with perido-

tite minerals and disappeared to form very potassic melts in all other runs. Analyses of the melts are listed in Table 3. Compared with melts of Runs #26–51, they are rich in K_2O and SiO_2 and depleted in MgO , FeO and CaO . The melt formed near the solidus of the potassic peridotite at 20 kbar (Run #60) contains normative nepheline, orthoclase and albite components, whereas the one at 30 kbar (Run #62) contains normative leucite instead of albite (Table 3). This observation is consistent with melting relations in the $KMAS$ system (Kushiro, 1980; Wendlandt and Egger, 1980) where the initial melts are very rich in potassic feldspar component and their normative compositions change from enstatite-bearing to leucite-bearing at about 20 kbar.

It is important to note that the solidus defined with the potassic peridotite approaches or might cross the normal oceanic geotherm (e.g., Clark and Ringwood, 1964; Pollack and Chapman, 1977) at pressures between 30 and 50 kbar (Fig. 9). The presence of volatiles (H_2O , CO_2) has been regarded as necessary to explain the Low Velocity Zones in the upper mantle by partial melting (Kushiro *et al.*, 1968; Lambert and Wyllie, 1968; Wyllie, 1973; Egger, 1976). The present observation, however, suggests an alternative possibility, that the earth's upper mantle can be partially molten under dry conditions even under a normal geothermal gradient only when it contains a substantial amount of potassium.

If the upper mantle contains 1000 ppm K_2O on the average (Ringwood, 1975), the degree of partial melting along the solidus of the peridotite would be on the order of 1 wt.%, judging from the K_2O content of the liquids in Table 3. Such a small amount of melt will not segregate from the peridotite matrix under hydrostatic conditions (Stolper *et al.*, 1981). The presence of 1 wt.% melt in the grain boundaries of peridotite, however, might account for the decrease in seismic wave velocities and their attenuation observed in the earth's Low Velocity Zones (Anderson and Sammis, 1970; Stocker and Gordon, 1975).

Potassic magmas represented by unusually high K_2O and K/Na ratio erupted at many localities in the world: oceanic islands, continental rift zones, and continental shields associated with kimberlites (e.g., see Gupta and Yagi, 1980). Despite the isolation of the activity in time and space, these magmas form a distinct and unique chemical and petrological province (Turner and Verhooogen, 1951; Wendlandt and Egger, 1980). Some of the potassic rocks relatively rich in silica (*i.e.*, leucite phonolite, leucite basalt) might represent the dry partial melts formed along the solidus shown in Figure 9.

The Fe/Mg partitioning between olivine and liquid

The partitioning of Fe and Mg between olivine and magmatic liquids has been studied extensively, and it has been demonstrated that $K_D(Fe/Mg)^{ol-liq} = (Fe/Mg)^{ol} / (Fe/Mg)^{liq}$ is nearly constant (0.30 ± 0.03) at one atmo-

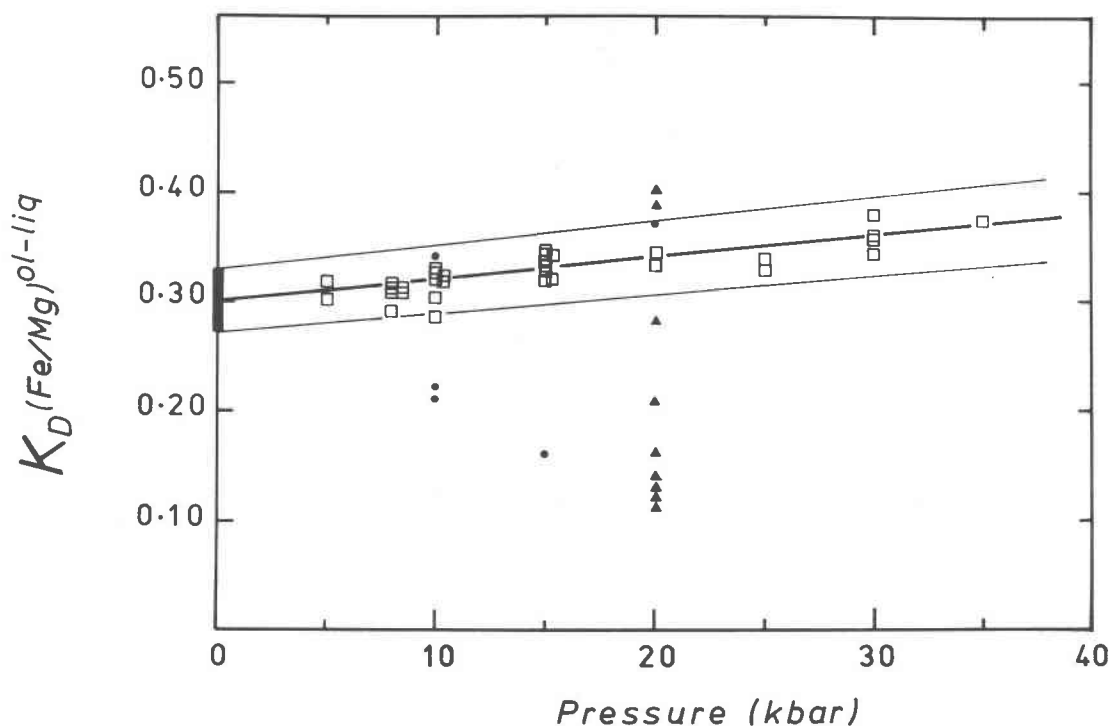


Fig. 10. The olivine-liquid Fe/Mg partition coefficient $K_D = (\text{Fe}/\text{Mg})^{\text{ol}}/(\text{Fe}/\text{Mg})^{\text{liq}}$ as a function of pressure (open squares). The range at one atmosphere (0.30 ± 0.03) is from Roeder and Emslie (1970). A slight positive trend with increasing pressure is seen; $K_D = 0.30 + 0.002 P$ (kbar). Small solid symbols indicate the K_D values obtained in previous melting studies of peridotite with direct EPMA analysis of quenched liquids: circles, Kushiro (1973b), triangles, Mysen and Kushiro (1977).

sphere over a large temperature interval and variety of liquid compositions (*e.g.*, Roeder and Emslie, 1970; Takahashi, 1978). Because of its importance in placing constraints on igneous petrogenesis, determination of K_D at high pressures is strongly needed. The present results can be used to test the pressure effect on the K_D values, inasmuch as compositions of olivine and coexisting liquids were measured over a large pressure interval. Chemical equilibrium between olivine and liquid is believed to have been established throughout the basalt melt and the peridotite layers (see Figs. 4 and 7). Ferric iron in the melt can be neglected because of the low oxygen fugacity imposed by the graphite container.

The K_D values calculated from the analysis of liquids and coexisting olivine (Table 3) are shown as a function of pressure in Figure 10. The K_D values show a positive trend with increasing pressure ($K_D = 0.30 + 0.002P$ kbar). Even though the K_D value is known to be insensitive to temperature and liquid compositions at 1 atm, it is not absolutely clear whether the increase in K_D at high pressures is due to the intrinsic pressure effect, because the experimental temperatures and liquid compositions are changing simultaneously with pressure, and the range of variation is much wider than those examined at 1 atm. Nevertheless, the trend is useful, because it gives the range in liquid compositions under pressure-temperature

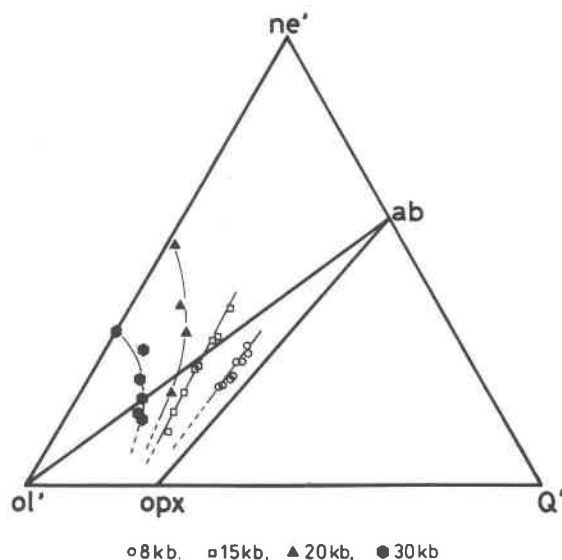


Fig. 11. Normative liquid compositions obtained with the basalt/peridotite sandwich technique (see Fig. 3). The same projection scheme to Figure 6. All the liquid compositions obtained at 8, 15, 20 and 30 kbar are plotted (Table 3). Isobaric liquid compositional trends (solid lines) extend toward ol-Q join so that they agree with the data in the system $\text{Mg}_2\text{SiO}_4\text{-SiO}_2$ by Chen and Presnall (1975).

conditions relevant to basalt magma genesis in the earth's upper mantle.

Also shown in Figure 10 are K_D values calculated from coexisting olivine and liquid reported in previous melting experiments on peridotite under dry conditions. The previous data are scattered and systematically lower than the trend obtained by the present experiments. As noted previously, the major reason for the discrepancy is that the liquid compositions reported in the previous studies have been modified considerably by quench crystallization (Fig. 1). In the present experiments we observed that the glasses in the peridotite matrix are heterogeneous in chemical composition regardless of run duration and are much poorer in MgO, lower in MgO/FeO and enriched in Al_2O_3 and SiO_2 than the liquids quenched in the glass disk in the same charge. These lines of evidence support the conclusion of Jaques and Green (1979) who claimed that chemical compositions of the peridotite partial melts are unquenchable in ordinary quenching experiments and that most previously reported compositions of the melts by direct EPMA analysis are greatly in error except those obtained near the center of large glass pods.

Based on peridotite melting experiments under hydrous conditions, Mysen (1975) reported that the K_D changes from 0.12 at 10 kbar to 0.30 at 30 kbar, at 1100°C and under oxygen fugacities close to the NNO buffer. As described above, however, his liquid compositions determined by direct EPMA analysis of quenched glass are subject to much doubt. Furthermore, it can also be argued that his unbuffered experiments with Ag-Pd containers gave oxygen fugacities which increased with run duration due to the alloying reaction of Fe in the container as noted previously. His liquids may, therefore, con-

tain much greater amounts of ferric iron than he expected after long runs. The amount of change in the oxygen fugacity is also dependent on the modal proportion of the melt to the container and on various physical properties (*e.g.*, cationic diffusion coefficients in melt); hence f_{O_2} is a complex function of pressure and temperature. Further experiments are necessary in order to clarify these points and to know the exact K_D values under hydrous conditions.

Isobaric liquid compositional trends and comparison with previous work

Compositions of melts obtained in this study are plotted on a ternary projection of the normative basalt tetrahedron (Fig. 11). Liquids within and close to the olivine tholeiite field of the basalt tetrahedron (Yoder and Tilley, 1962) are also plotted in the Walker's ternary projections (Fig. 12A,B) which have been used for discussion of mid-ocean ridge basalt (MORB) petrogenesis (Walker *et al.*, 1979; Stolper, 1980). In those ternary projections, liquids obtained at each pressure lie along a single line.

In a four component system such as CMAS (CaO-MgO- Al_2O_3 - SiO_2), liquids coexisting with three solid phases at a given pressure are univariant, hence they must lie on a single line in ternary projections similar to Figures 11 and 12. Liquids coexisting only with two solid phases, however, need not lie along such isobaric liquidus boundaries in the ternary projections. In the case of natural peridotite, melts formed after extensive partial melting contain only small amounts of clinopyroxene and feldspar components. In other words, melts leaving a harzburgite residue may differ only slightly in chemical composition at a given

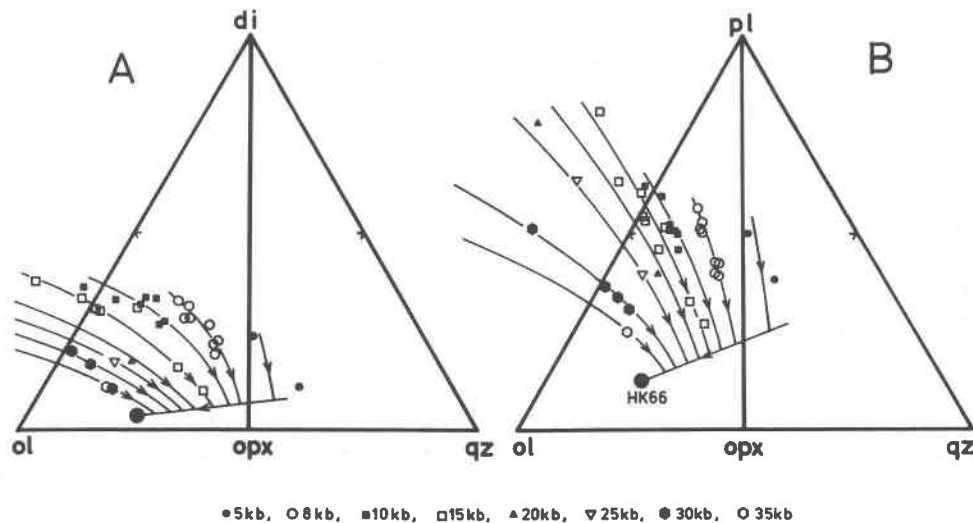


Fig. 12. Normative liquid compositions and the isobaric liquid compositional trends in ternary projections by Walker *et al.* (1979). A, projection from plagioclase onto the plane olivine–diopside–quartz; B, projection from diopside to olivine–plagioclase–quartz. Liquids projected far away from the normative triangle were omitted (*cf.*, Fig. 11 with Fig. 12B).

pressure-temperature condition even if they started from different lherzolite sources. The trends defined in Figures 11 and 12, which refer to liquids coexisting with the three solid phases near the solidus and the liquids coexisting only with olivine and orthopyroxene at higher temperatures, thus are considered to be a good approximation of isobaric liquid trends on which most of the peridotite partial melts are located.

In all the ternary projections, the location of the isobaric liquid trends shifts systematically toward the olivine apex as pressure increases (Figs. 11 and 12). In other words, a peridotite partial melt formed at higher pressure is invariably more enriched in normative olivine compared to the melt formed at a lower pressure and at a similar ΔT from the solidus.

In his classic reviews, O'Hara (1965, 1968) estimated the initial melt composition of natural peridotite as a function of pressure. The present observations show general agreement with his estimation in that the liquids obtained at higher pressures are more olivine rich than those at lower pressures. They support O'Hara's view that the initial melt formed at pressures above 15 kbar are alkali basalts. O'Hara expected that the initial melt returns to the olivine tholeiite field (the ol-opx-di and pl-opx triangles in Fig. 12) at some pressure below 30 kbar (O'Hara, 1965, Fig. 14). In the present study, however, the initial melt at 30 kbar turns out to be a very silica undersaturated potassic melt (leucite phonolite, see

Fig. 11). Based on the systematics in our experimental observations and their good consistency with experimental results in simple oxide systems such as KMAS (Kushiro, 1980; Wendlandt and Egger, 1980) and NMAS (Kushiro, 1968), it is concluded that the initial peridotite melt becomes increasingly alkalic and silica undersaturated as pressure increases at least up to 30 kbar.

In the CMAS system simulating peridotite, Presnall *et al.* (1979) estimated initial melt compositions as a function of pressure. Their estimated liquid compositions were plotted in Figure 13. Compared with the solidus melts in the CMAS system, the compositions of the melts formed along the solidus of HK66 are systematically silica deficient. This must be due to the presence of alkalis in the natural rocks used in this study. Hoover and Presnall (1982) have carried out melting experiments in the NCMAS system ($\text{Na}_2\text{O}-\text{CaO}-\text{MgO}-\text{Al}_2\text{O}_3-\text{SiO}_2$). According to them the compositions of the solidus melts in the NCMAS system are more silica deficient than in CMAS, and the locations of the isobaric liquid trends virtually coincide with those of the present study (Hoover and Presnall, 1982; and also D. C. Presnall, pers. comm., 1982).

Using the same basalt/peridotite sandwich technique, Fujii and Scarfe (1981) have studied the effect of bulk chemical composition of the source peridotite on the composition of the partial melts at 10 kbar. According to them, melts coexisting with olivine + orthopyroxene + clinopyroxene of more magnesian compositions than

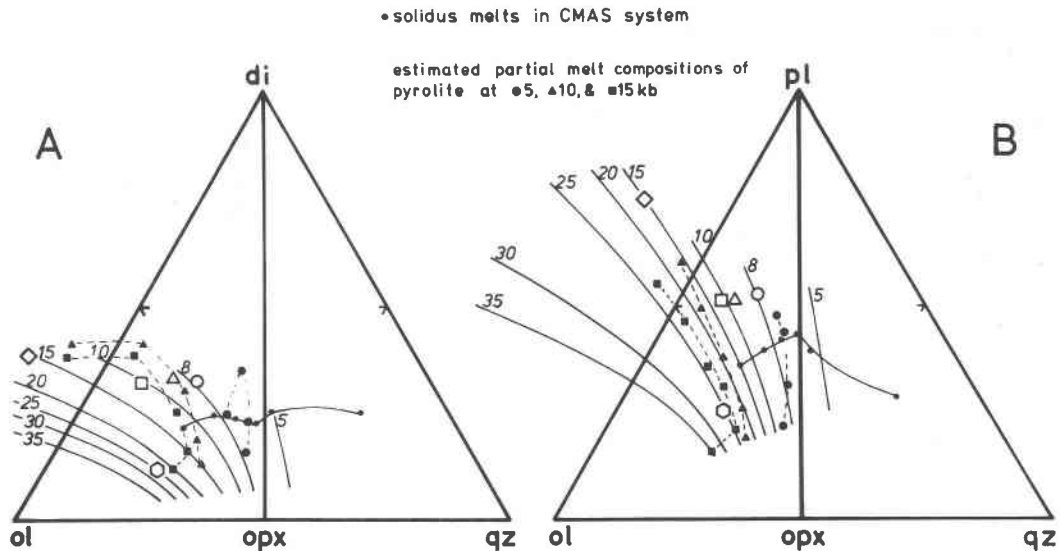


Fig. 13. Comparison of our isobaric liquid compositional trends with previous work. Projection is the same as in Fig. 12. Small solid circles with light-solid lines show compositions of isobaric invariant points in the CMAS system at 1 atm, 7, 9.3, 11, 14, and 20 kbar from qz-rich side toward ol-rich side (Presnall *et al.*, 1979). Solid symbols with broken lines denote isobaric liquid compositional trends of a pyrolite estimated by mass balance calculation by Jaques and Green (1980). Open symbols show compositions of natural basaltic rocks which are experimentally demonstrated to coexist with olivine + orthopyroxene + clinopyroxene at following conditions: (circle) MORB, 7.5 kbar, 1210°C, Kushiro (1973a); (triangle) MORB, 8 kbar, 1225°C, Fujii and Kushiro (1977); (square) MORB, 11 kbar, 1290°C, Bender *et al.* (1978); (diamond) alkali-olivine basalt, 14 kbar, 1275°C, Takahashi (1980c); (hexagon) picrite, 25 kbar, 1470°C, Elthon and Scarfe (1980).

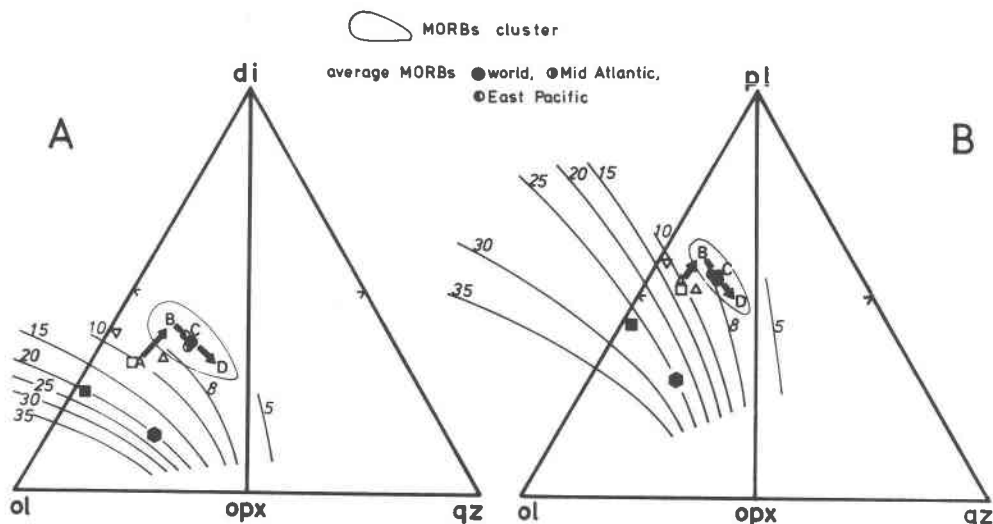


Fig. 14. A schematic diagram illustrating a model for generation of MORBs from a peridotite partial melt formed at 10 kbar and 1275°C (point A). The areas of the MORBs' main cluster from Walker *et al.* (1979) and Stolper (1980). The average MORBs compositions from Melson *et al.* (1976). Other symbols; (normal triangle) the most magnesian glass from Leg. 45, Fujii and Kushiro (1977); (open square) the most magnesian glass from the FAMOUS area, Bender *et al.* (1978); (inverted triangle) average olivine-phyric tholeiite from Leg. 37, Irvine (1979); (solid square) estimated primary magma for MORBs by an olivine fractionation model, Irvine (1979); (solid hexagon) estimated primary picrite magma for MORBs, Elthon and Scarfe (1980).

those of the present study ($Mg/(Mg+Fe) = 0.88-0.93$) are slightly more enriched in both MgO and CaO (10–13 wt.%, and 11–13 wt.%, respectively) than those listed in Table 3. Their liquid compositions in the CIPW normative projections, however, are very close to the 10 kbar liquid trends shown in Figure 12. Based on the concordance with the experiments by Fujii and Scarfe (1981) and Hoover and Presnall (1982), it is anticipated that the isobaric liquid trends in Figure 12 are valid for peridotites with $Mg/(Mg+Fe)$ from 0.85 through 1.0.

Jaques and Green (1980) estimated liquid compositions in anhydrous melting studies of synthetic peridotites. Their liquid compositions are compared with our results in Figure 13. In the ol-pl-Q projection (Fig. 13B), agreement of the two results is relatively good but the liquids of Jaques and Green are considerably richer in normative diopside relative to ours in the ol-di-Q diagram (Fig. 13A). The liquids of Jaques and Green (1980) are also systematically lower in Al_2O_3 than ours (by about 2 to 3 wt.%) when compared at the same ΔT from the solidus at a given pressure. A possibility that might account for the discrepancy is in the uncertainty of the estimation of the liquid compositions by Jaques and Green (1980) based on chemical compositions and modes of solid residues. Clinopyroxenes in their run products revealed compositional zoning (Jaques and Green, 1980, p. 298), and they tentatively assumed the most calcic and low alumina clinopyroxene as equilibrium compositions. It is likely, however, that their pyroxene compositions are metastable because of short run durations (see Figs. 2, 4 and Table 4).

Stolper (1980) has made melting experiments with an abyssal tholeiite using harzburgite as a container. With

liquid compositions which are coexisting with olivine + orthopyroxene or olivine + orthopyroxene + clinopyroxene, and assuming that the composition of the liquid coexisting with the latter three minerals is pseudoinvariant at a given pressure, he constructed polybaric phase diagrams for MORBs. However, it is clear from the present study and also that of Fujii and Scarfe (1981) that the liquids coexisting with olivine + orthopyroxene + clinopyroxene can not be treated as pseudoinvariant points and the compositions of those liquids range toward more silica deficient portions of the diagram than he considered (*cf.* Fig. 12 with Stolper's Figs. 2 and 3).

Compositions of basalts which are experimentally demonstrated to coexist with olivine + orthopyroxene + clinopyroxene at certain pressure-temperature conditions are plotted in Figure 13. The experimentally bracketed pressures for those basalts are in excellent agreement with the isobaric liquid compositional trends defined by the present study. Based on the above observations, it may be argued that we have shown a general set of isobaric liquid trends in Figure 12 and the dry basaltic melts formed by partial melting of mantle peridotite are plotted on the trend at their depth of last equilibration with the upper mantle. And it follows that we may be able to estimate the depth of segregation of a basalt magma from its chemical composition by fitting the isobaric liquid trends in Figure 12. An example of such an application is illustrated below.

Genesis of MORBs from dry peridotite

The origin of mid-ocean ridge basalts (MORBs) is a subject of much debate (*e.g.*, O'Hara, 1968; Green, 1971;

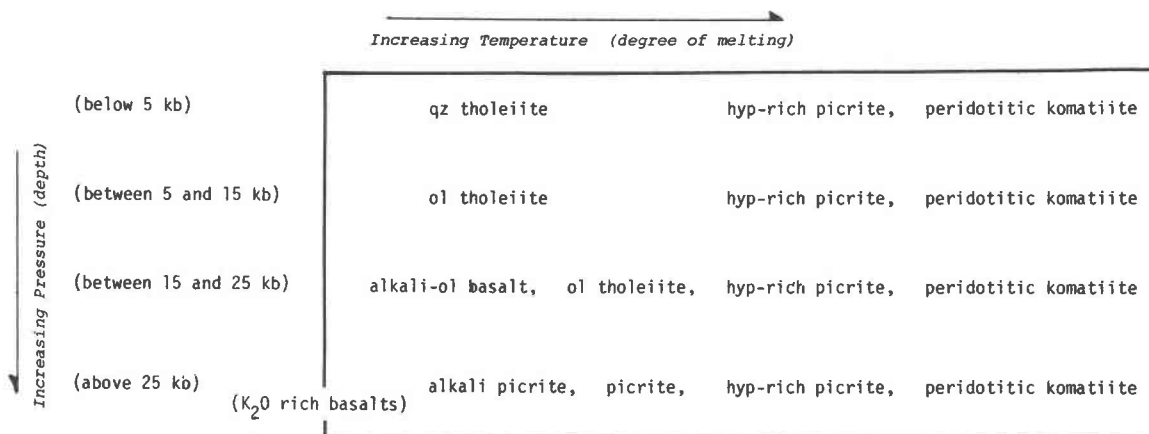


Fig. 15. A petrogenetic grid showing the compositional diversity of basaltic magmas formed by partial melting of dry peridotite at various pressure and temperature conditions.

Kushiro, 1973a; Presnall *et al.*, 1979; Stolper, 1980; Elthon and Scarfe, 1980). An important consensus exists, however, among petrologists and geochemists that most fresh MORBs contain very little water and other volatile constituents (Moore, 1970; Delaney *et al.*, 1978). Experimentally determined phase relations at high pressures under dry conditions, therefore, are directly applicable for petrogenesis of MORBs. It has been demonstrated experimentally that some magnesian MORBs coexist simultaneously with olivine + orthopyroxene + clinopyroxene at pressures of 7 to 11 kbar (Kushiro, 1973a; Fujii and Kushiro, 1977; Bender *et al.*, 1978; see Figure 13 for normative compositions of the basalts), whereas other authors have failed to find such a relation using similar MORB compositions (*e.g.*, Green *et al.*, 1979).

Based on experimental results in the CMAS system, Presnall *et al.* (1979) predicted that initial melts of natural peridotite at a pressure of about 9 kbar are close to the composition field of the least fractionated MORBs (see Fig. 13). Hoover and Presnall (1982) supported the above prediction based on their experimental results in the NCMAS system. On the other hand, Jaques and Green (1980) and Stolper (1980) concluded that peridotite partial melts formed at about 10 kbar are notably different from the typical MORBs based on their experiments discussed previously. They proposed high pressure origins for the MORBs.

The present experiments have shown that initial melt compositions formed near the solidus of the peridotite HK66 at 8 kbar are rich in Al₂O₃ and CaO (about 16 and 11 wt.%, respectively), moderate in SiO₂ (49–50 wt.%), olivine normative (about 10 mole %) and poor in K₂O. These liquids are virtually indistinguishable from the most typical MORBs that cluster in the center of the MORB's variation (Fig. 14). At 10 kbar, the initial melt composition becomes more silica deficient, olivine rich and away from the main MORBs cluster. Compositions of the magnesian variety of the MORBs, however, fall close

to our liquid trend at 10 kbar (open symbols in Fig. 14A,B). Furthermore, it is important to note that overall compositional variations of the MORBs could be produced from the melts formed at 10 kbar in the following way.

If a magma produced at 10 kbar and 1275°C (point A in Fig. 14) rose and underwent fractional crystallization in a near surface magma chamber, the first phase to crystallize would be olivine (O'Hara, 1968). At point B, clinopyroxene and plagioclase begin to crystallize together with olivine, and the composition of the liquid would follow the path B to C and then to D (Walker *et al.*, 1979). In the same way, the variety of MORBs could be produced by fractional crystallization in a shallow magma chamber starting from peridotite partial melts formed at any pressure above 10 kbar. It is emphasized, however, that the magmas produced at 8 and 10 kbar by partial melting need only a very small amount of crystallization to become typical MORBs.

The Mg-value (100Mg/(Mg+Fe²⁺)) of typical MORBs are in the range between 50 and 70 and their magnesian variety contains 200–250 ppm Ni (*e.g.*, Schilling *et al.*, in press). Using the K_D partition coefficients between olivine and liquid, 0.32 for Fe–Mg at 10 kbar (Fig. 10, this study) and 2.3 for Ni–Mg at 10 kbar (Takahashi, 1980a), compositions of olivines in equilibrium with the MORBs at 10 kbar can be calculated. According to the above calculation, a MORB with Mg-value 70, 10 wt.% MgO and 250 ppm Ni would coexist with olivine of Fo₈₈ and 0.35 wt.% NiO on its liquidus at 10 kbar. The above olivine composition is within the compositional range of olivines in mantle peridotites (*e.g.*, see Fig. 2 of Sato, 1977). In fact, such magnesian olivine phenocrysts or xenocrysts (Fo_{88–90}) often have been reported from normal magnesian MORBs (*e.g.*, Frey *et al.*, 1974). Whether the magnesian MORBs actually are direct partial melt products or have undergone a small amount of low pressure fractionation needs further clarification. But it is less likely that they have evolved from picritic primary magmas after

extensive olivine fractionation (O'Hara, 1968; Irvine, 1979; Green *et al.*, 1979; Elthon and Scarfe, 1980), because such olivine fractionation would have eliminated nickel from the magmas (Sato, 1977; Hart and Davis, 1978).

Compositional diversity of magmas formed by partial melting of dry peridotite

Based on the present experimental results a petrogenetic grid was constructed illustrating the compositional diversity of magmas formed by partial melting of dry peridotite at pressures of 5 to 30 kbar (Fig. 15). Along the solidus of dry peridotite, a variety of basalts such as quartz tholeiite, olivine tholeiite, alkali-olivine basalt and alkali picrite are produced. Very potassic magmas equivalent to leucite basalt and leucite phonolite can be produced at relatively low temperatures (1300–1400°C) in the pressure range above about 20 kbar. The amount of such potassic melt, however, is strongly dependent on the K_2O content of the peridotite. In the case of peridotite depleted in alkalis, only picritic tholeiite melt could be produced in appreciable amount at pressures above 25 kbar.

A very silica deficient variety of alkali- mafic magmas (basanite, melilitite, nephelinite), however, can not be derived from dry peridotite by partial melting alone. The lowest SiO_2 value of the liquid obtained in our experiments is 46.5 wt.% (Run #47). Thus, the highly silica-deficient magmas may be partial melt products of peridotite with CO_2 (Eggler, 1978; Wendlandt and Mysen, 1980).

High-alumina basalts (occasionally with 18 wt.% Al_2O_3 or more) which occur in island-arcs and continental margins have been identified as a primary basalt magma type (Kuno, 1960). Compared to the liquids of the present study, they are closest to the solidus melt at 8 to 15 kbar except that Kuno's high-alumina basalts are more enriched in normative plagioclase components. The high-alumina basalts in the oceanic belts subduction zones may be partial melt products of peridotite under slightly wet conditions (Takahashi *et al.*, 1981).

Conclusions

(1) The solidus curve of a dry peridotite HK66 has cusps at points where the subsolidus phase assemblage changes, and it is lower in temperature by about 100°C than previously determined.

(2) Along the solidus the composition of partial melt of the peridotite changes; quartz tholeiite at 5 kbar, olivine tholeiite at 8 and 10 kbar, alkali-olivine basalt at 15 and 20 kbar, and alkali picrite at 25 and 30 kbar.

(3) Addition of potassium feldspar component to the peridotite, lowers the dry solidus significantly, and its extension might intersect the normal oceanic geotherm at pressures between 30 and 50 kbar. The solidus curve of the potassic peridotite is considered to be the true dry solidus of the earth's upper mantle.

(4) At temperatures between the two solidi, a variety of potassic magmas such as leucite phonolite and leucite basalt are produced as incipient melt of dry mantle peridotite.

(5) The olivine/liquid Fe–Mg partition coefficient shows a slight positive trend with increasing pressure $K_D = 0.30 + 0.002 P$ (kbar). Judging from the K_D values, most previously reported glass compositions in peridotite melting experiments by direct EPMA analysis are considerably in error.

(6) In normative projections, isobaric liquid compositional trends have been defined based on the present experiments. The isobaric trends shift systematically toward the olivine apex as pressure increases and the initial melt compositions become increasingly silica-deficient. These trends are consistent with previous melting studies in synthetic systems and those with natural basalts.

(7) The partial melting model of mantle peridotite at pressures of 8 to 10 kbar for origin of MORBs is supported, both because compositions of the melts formed near the solidus at above pressures are very close to typical magnesian MORBs and because the observed diversity of the MORBs can be produced from the partial melts by fractional crystallization at shallower depths.

Acknowledgments

We are grateful to Dr. H. S. Yoder, Jr., director of the Geophysical Laboratory, Carnegie Institution of Washington, where most of the present experiments were made. We are thankful to Drs. F. R. Boyd and B. O. Mysen of the Geophysical Laboratory for providing their experimental facilities. Special thanks are due to Drs. T. N. Irvine, A. Navrotsky, and D. C. Presnall who contributed greatly to improve the manuscript by careful review. We also appreciate criticisms and comments on the manuscript by Drs. F. Chayes, P. A. Danckwerth, T. Fujii, M. J. Holdaway, S. Jakobsson, A. L. Jaques, Y. Matsui, and C. M. Scarfe at various stages of its preparation. Thanks are also due to Mr. C. G. Hadidiacos who assisted the electron microprobe work.

References

- Anderson, D. L. and Sammis, C. (1970) Partial melting in the upper mantle. *Physics of the Earth and Planetary Interiors*, 3, 41–50.
- Bender, J. F., Hodges, F.N. and Bence, A. E. (1978) Petrogenesis of basalts from the project FAMOUS area: experimental study from 0 to 15 kbars. *Earth and Planetary Science Letters*, 41, 277–302.
- Bowen, N. L. (1913) Melting phenomenon of plagioclase feldspar. *American Journal of Science* (4th series), 35, 577–599.
- Bowen, N. L. (1928) *The Evolution of the Igneous Rocks*. Princeton University Press, New Jersey.
- Boyd, F. R. and England, J. L. (1960) Apparatus for phase-equilibrium measurements at pressures to 50 kilobars and temperatures up to 1750°C. *Journal of Geophysical Research*, 65, 741–748.
- Chen, C. H. and Presnall, D. C. (1975) The system Mg_2SiO_4 –

- SiO₂ at pressures up to 25 kilobars. *American Mineralogist*, 60, 398–406.
- Clark, S. P. and Ringwood, A. E. (1964) Density distribution and constitution of the mantle. *Review in Geophysics*, 2, 35–88.
- Crank, J. (1956) *The Mathematics of Diffusion*. Oxford University Press, London.
- Delaney, J. R., Muenow, D. W. and Graham, D. G. (1978) Abundance and distribution of water, carbon and sulfur in the glassy rims of submarine pillow basalts. *Geochimica et Cosmochimica Acta*, 42, 581–594.
- Eggler, D. H. (1976) Does CO₂ cause partial melting in the low velocity layer of the mantle? *Geology*, 4, 69–72.
- Eggler, D. H. (1978) The effect of CO₂ upon partial melting of peridotite in the system Na₂O–CaO–Al₂O₃–MgO–SiO₂–CO₂ to 35 kb, with an analysis of melting in a peridotite–H₂O–CO₂ system. *American Journal of Science*, 278, 305–343.
- Elthon, D. and Scarfe, C. M. (1980) High-pressure phase equilibria of a high-magnesia basalt: implications for the origin of mid-ocean ridge basalts. *Carnegie Institution of Washington Year Book*, 79, 277–281.
- Erlank, A. J. and Kushiro, I. (1970) Potassium contents of synthetic pyroxenes at high temperatures and pressures. *Carnegie Institution of Washington Year Book*, 68, 233–236.
- Frey, F. A., Bryan, W. B. and Thompson, G. (1974) Atlantic ocean floor: Geochemistry and petrology of basalts from Leg 2 and 3 of the Deep-Sea Drilling Project. *Journal of Geophysical Research*, 79, 5507–5527.
- Fujii, T. and Kushiro, I. (1977) Melting relations and viscosity of an abyssal tholeiite. *Carnegie Institution of Washington Year Book*, 76, 461–465.
- Fujii, T. and Scarfe, C. M. (1981) Partial melting of spinel lherzolite and its bearing on the origin of MORBs. (abstr.) *Geological Society of America Abstracts with Programs*, 13, 456.
- Green, D. H. (1971) Compositions of basaltic magmas as indicators of conditions of origin: application to oceanic volcanism. *Philosophical Transactions of the Royal Society of London*, 268a, 707–725.
- Green, D. H. (1973) Experimental melting studies on a model upper mantle composition at high pressure under water-saturated and water-undersaturated conditions. *Earth and Planetary Science Letters*, 19, 37–53.
- Green, D. H. and Ringwood, A. E. (1967a) The genesis of basaltic magmas. *Contributions to Mineralogy and Petrology*, 15, 103–190.
- Green, D. H. and Ringwood, A. E. (1967b) The stability of aluminous pyroxene peridotite and garnet peridotite and their relevance in upper mantle structure. *Earth and Planetary Science Letters*, 3, 151–160.
- Green, D. H., Hibberson, W. O. and Jaques, A. L. (1979) Petrogenesis of mid-ocean ridge basalts. In M. W. McElhinny, Ed., *The Earth: Its Origin, Structure and Evolution*, p. 265–299. Academic Press, London.
- Gupta, A. K. and Yagi, K. (1980) *Petrology and Genesis of Leucite-bearing Rocks*. Springer-Verlag.
- Hart, S. R. and Davis, K. E. (1978) Nickel partitioning between olivine and silicate melt. *Earth and Planetary Science Letters*, 40, 203–219.
- Hofmann, A. W. (1980) Diffusion in natural silicate melts: a critical review. In R. B. Hargraves, Ed., *Physics of Magmatic Processes*, p. 385–418. Princeton University Press, New Jersey.
- Hoover, J. D. and Presnall, D. C. (1982) Melting relations of simplified peridotite in the SiO₂–CaO–Al₂O₃–MgO–Na₂O (SCAMN) system from 1 atm to 20 kb-II. Results and application to basalt generation. (abstr.) *Geological Society of America Abstracts with Programs*, 14, 517.
- Irvine, T. N. (1977) Chromite crystallization in the join Mg₂SiO₄–CaMgSi₂O₆–CaAl₂Si₂O₈–MgCr₂O₄–SiO₂. *Carnegie Institution of Washington Year Book*, 76, 465–472.
- Irvine, T. N. (1979) Rocks whose composition is determined by crystal accumulation and sorting. In H. S. Yoder Jr., Ed., *The Evolution of the Igneous Rocks*, p. 245–306. Princeton University Press, New Jersey.
- Irvine, T. N. and Baragar, W. R. A. (1971) A guide to the chemical classification of the common volcanic rocks. *Canadian Journal of Earth Sciences*, 8, 523–548.
- Ito, K. and Kennedy, G. C. (1968) Melting and phase relations in the plane tholeiite–lherzolite–nepheline basanite to 40 kilobars with geological implications. *Contributions to Mineralogy and Petrology*, 19, 177–211.
- Jaques, A. L. and Green, D. H. (1979) Determination of liquid compositions in experimental, high pressure melting of peridotite. *American Mineralogist*, 64, 1312–1321.
- Jaques, A. L. and Green, D. H. (1980) Anhydrous melting of peridotite at 0–15 kb pressure and the genesis of tholeiitic basalts. *Contributions to Mineralogy and Petrology*, 73, 287–310.
- Kuno, H. (1960) High-alumina basalt. *Journal of Petrology*, 1, 121–145.
- Kushiro, I. (1968) Composition of magmas formed by partial zone melting of the earth's upper mantle. *Journal of Geophysical Research*, 73, 619–634.
- Kushiro, I. (1973a) Origin of some magmas in oceanic and circum-oceanic regions. *Tectonophysics*, 17, 211–222.
- Kushiro, I. (1973b) Partial melting of garnet lherzolites from kimberlite at high pressures. In P. H. Nixon, Ed., *Lesotho Kimberlites*, p. 294–299. National Development Corporation, Lesotho.
- Kushiro, I. (1974) Melting of hydrous mantle and possible generation of andesitic magma: an approach from synthetic systems. *Earth and Planetary Science Letters*, 22, 294–299.
- Kushiro, I. (1975) On the nature of silicate melt and its significance in magma genesis: regularities in the shift of the liquidus boundaries involving olivine, pyroxene and silica minerals. *American Journal of Science*, 275, 411–431.
- Kushiro, I. (1976) A new furnace assembly with a small temperature gradient in solid-media, high-pressure apparatus. *Carnegie Institution of Washington Year Book*, 75, 832–833.
- Kushiro, I. (1980) Changes with pressure of degree of partial melting and K₂O content of liquids in the system Mg₂SiO₄–KAlSiO₄–SiO₂. *Carnegie Institution of Washington Year Book*, 79, 267–271.
- Kushiro, I. and Kuno, H. (1963) Origin of primary basalt magmas and classification of basaltic rocks. *Journal of Petrology*, 4, 75–89.
- Kushiro, I., Syono, Y. and Akimoto, S. (1968) Melting of a peridotite nodule at high pressures and high water pressures. *Journal of Geophysical Research*, 73, 6023–6029.
- Kushiro, I., Shimizu, N., Nakamura, Y. and Akimoto, S. (1972) Compositions of coexisting liquid and solid phases formed upon melting of natural garnet and spinel lherzolites at high pressures: A preliminary report. *Earth and Planetary Science Letters*, 14, 19–25.

- Lambert, I. B. and Wyllie, P. J. (1968) Stability of hornblende and a model for the low velocity zone. *Nature*, 219, 1240–1241.
- Lindsley, D. H. (1980) Phase equilibria of pyroxenes at pressures >1 atmosphere. In C. T. Prewitt, Ed., *Reviews in Mineralogy*, 7, Pyroxenes, p. 289–308. Mineralogical Society of America, Washington D.C.
- McCallister, R. H. (1980) Determinations of major cationic diffusion constants in pyroxenes. (abstr.) *Geological Society of America Abstracts with Programs*, 13, 479.
- Melson, W. G., Vallier, T. L., Wright, T. L., Byerly, G. and Nelen, J. (1976) Chemical diversity of abyssal volcanic glass erupted along Pacific, Atlantic, and Indian ocean spreading centers. In G. H. Sutton *et al.*, Eds., *Geophysical Monograph*, 19, The Geophysics of the Pacific Ocean Basin and its Margin, p. 351–367. American Geophysical Union, Washington D.C.
- Misener, D. J. (1974) Cationic diffusion in olivine to 1400°C and 35 kilobars. In A. W. Hofmann, Ed., *Geochemical Transport and Kinetics*, p. 117–129. Carnegie Institution of Washington, Washington D.C.
- Moore, J. G. (1970) Water content of basalt erupted on the ocean floor. *Contributions to Mineralogy and Petrology*, 28, 272–279.
- Morioka, M. (1981) Cation diffusion in olivine-II, Ni–Mg, Mn–Mg, Mg and Ca. *Geochimica et Cosmochimica Acta*, 45, 1573–1580.
- Mysen, B. O. (1975) Partitioning of iron and magnesium between crystal and melts in peridotite upper mantle. *Contributions to Mineralogy and Petrology*, 52, 69–76.
- Mysen, B. O. and Boettcher, A. L. (1975) Melting of a hydrous upper mantle: II, Geochemistry of crystal and liquids formed by anatexis of mantle peridotite at high pressure and high temperatures as a function of controlled activities of water, hydrogen, and carbon dioxide. *Journal of Petrology*, 16, 549–593.
- Mysen, B. O. and Kushiro, I. (1977) Compositional variations of coexisting phases with degree of melting of peridotite in the upper mantle. *American Mineralogist*, 62, 843–865.
- O'Hara, M. J. (1965) Primary magmas and the origin of basalts. *Scottish Journal of Geology*, 1, 19–40.
- O'Hara, M. J. (1968) The bearing of phase equilibria studies in synthetic and natural systems on the origin and evolution of basic and ultrabasic rocks. *Earth-Science Review*, 4, 69–134.
- Pollack, H. N. and Chapman, D. S. (1977) On the regional variation of heat flow, geotherms, and lithospheric thickness. *Tectonophysics*, 38, 279–296.
- Presnall, D. C. and Brenner, N. L. (1974) A method for studying iron silicate liquids under reducing conditions with negligible iron loss. *Geochimica et Cosmochimica Acta*, 38, 1785–1788.
- Presnall, D. C. and Hoover, J. D. (1982) Melting relations of simplified peridotite in the $\text{SiO}_2\text{-CaO-Al}_2\text{O}_3\text{-MgO-Na}_2\text{O}$ (SCAMN) system from 1 atm to 20 kb-I. *Methodology*. (abstr.) *Geological Society of America Abstracts with Programs*, 14, 593.
- Presnall, D. C., Dixon, J. R., O'Donell, T. H. and Dixon, S. A. (1979) Generation of mid-ocean ridge tholeiites. *Journal of Petrology*, 20, 3–35.
- Ringwood, A. E. (1975) *Composition and Petrology of the Earth's Mantle*. McGraw-Hill, New York.
- Roeder, P. L. and Emslie, R. F. (1970) Olivine-liquid equilibrium. *Contributions to Mineralogy and Petrology*, 29, 275–289.
- Sato, H. (1977) Nickel content of basaltic magma: identification of primary magmas and measure of the degree of olivine fractionation. *Lithos*, 10, 113–120.
- Schilling, J.-G., Zajac, M., Evans, R., Johnston, T., White, W., Devine, J. D. and Kingsley, R. (in press) Petrologic and geochemical variations along the Mid-Atlantic Ridge from 29°N to 73°N. *American Journal of Science*.
- Shiraki, K. and Kuroda, N. (1977) The boninite revisited. *Journal of Geography*, Tokyo Geographical Society, 86, 174–190 (in Japanese).
- Stocker, R. L. and Gordon, R. B. (1975) Velocity and internal friction in partial melts. *Journal of Geophysical Research*, 80, 4828–4836.
- Stolper, E. (1980) A phase diagram for mid-ocean ridge basalts: preliminary results and implications for petrogenesis. *Contributions to Mineralogy and Petrology*, 74, 13–27.
- Stolper, E., Walker, D., Harger, B. H. and Hays, J. F. (1981) Melt segregation from partially molten source regions: the importance of melt density and source region size. *Journal of Geophysical Research*, 86, 6261–6271.
- Takahashi, E. (1978) Partitioning of Ni^{2+} , Co^{2+} , Fe^{2+} , Mn^{2+} and Mg^{2+} between olivine and silicate melts: compositional dependence of partition coefficient. *Geochimica et Cosmochimica Acta*, 42, 1829–1844.
- Takahashi, E. (1980a) Olivine/liquid nickel partitioning at high pressures: experiments with an olivine capsule (abstr.) *EOS*, Transaction of the American Geophysical Union, 61, 397.
- Takahashi, E. (1980b) Thermal history of lherzolite xenoliths-I, Petrology of lherzolite xenoliths from the Ichinomegata crater, Oga peninsula, Northeast Japan. *Geochimica et Cosmochimica Acta*, 44, 1643–1658.
- Takahashi, E. (1980c) Melting relations of an alkali-olivine basalt to 30 kbar and their bearing on the origin of alkali basaltic magmas. *Carnegie Institution of Washington Year Book*, 79, 271–276.
- Takahashi, E., Kushiro, I. and Tatsumi, Y. (1981) Melting of a peridotite at high pressures and its bearing on island arc magmas. (abstr.) *International Association of Volcanology and Chemistry of the Earth's Interior*, p. 365–366, Tokyo.
- Takahashi, E., Yamada, H. and Ito, E. (1982) A new furnace assembly to 100 kbar and 1500°C with minimum temperature uncertainty. *Geophysical Research Letters*, 9, 805–807.
- Thompson, R. N. and Kushiro, I. (1972) The oxygen fugacity within graphite capsules in piston-cylinder apparatus at high pressures. *Carnegie Institution of Washington Year Book*, 71, 615–616.
- Tsuchiyama, A. and Takahashi, E. (in press) Melting kinetics of a plagioclase feldspar. *Contribution to Mineralogy and Petrology*.
- Turner, F. J. and Verhoogen, J. (1951) *Igneous Petrology*. McGraw-Hill, New York.
- Walker, D., Shibata, T. and DeLong, S. E. (1979) Abyssal tholeiites from the Oceanographer fracture zone. II, Phase equilibria and mixing. *Contributions to Mineralogy and Petrology*, 70, 111–125.
- Watson, E. B. and Bender, J. F. (1980) Diffusion of cesium, samarium, strontium and chlorine in molten silicate at high temperatures and pressures. (abstr.) *Geological Society of America Abstracts with Programs*, 13, 545.
- Wendlandt, R. F. and Egger, D. H. (1980) The origins of potassic magmas: I, Melting relations in the systems $\text{KAlSiO}_4\text{-Mg}_2\text{SiO}_4\text{-SiO}_2$ and $\text{KAlSiO}_4\text{-MgO-SiO}_2\text{-CO}_2$ to 30 kilobars. *American Journal of Science*, 280, 385–420.
- Wendlandt, R. F. and Mysen, B. O. (1980) Melting phase relations of natural peridotite + CO_2 as a function of degree of melting at 15 and 30 kbar. *American Mineralogist*, 65, 37–44.

- Wyllie, P. J. (1973) Experimental petrology and global tectonics—A preview. *Tectonophysics*, 17, 189–209.
- Yoder, H. S. Jr. (1976) Generation of Basaltic Magma. National Academy of Science, Washington D.C.
- Yoder, H. S. Jr. and Tilley, C. E. (1962) Origin of basalt

magmas: an experimental study of natural and synthetic systems. *Journal of Petrology*, 3, 342–532.

*Manuscript received, June 17, 1982;
accepted for publication, February 28, 1983.*